A vector-based strategy for olfactory navigation in *Drosophila*

Andrew F. Siliciano[1,2], Sun Minni[1,3], Chad Morton[1,2], Charles K. Dowell[2], Noelle B. Eghbali[2], Juliana Y. Rhee[2] L.F. Abbott[3] and Vanessa Ruta[2*]

[1]These authors contributed equally to this work
[2] Laboratory of Neurophysiology and Behavior and Howard Hughes Medical Institute, The Rockefeller University, New York, NY, USA
[3]Mortimer B. Zuckerman Mind Brain Behavior Institute, Kavli Institute for Brain Science, Department of Neuroscience, Columbia University, New York, NY, USA

1 **Odors serve as essential cues for navigation. Although tracking an odor plume has been modeled as a**
2 **reflexive process, it remains unclear whether animals can use memories of their past odor encounters**
3 **to infer the spatial structure of their chemical environment or their location within it. Here we**
4 **developed a virtual-reality olfactory paradigm that allows head-fixed *Drosophila* to navigate structured**
5 **chemical landscapes, offering insight into how memory mechanisms shape their navigational strategies.**
6 **We found that flies track an appetitive odor corridor by following its boundary, alternating between**
7 **rapid counterturns to exit the plume and directed returns to its edge. Using a combination of behavioral**
8 **modeling, functional calcium imaging, and neural perturbations, we demonstrate that this 'edge-**
9 **tracking' strategy relies on vector-based computations within the *Drosophila* central complex in which**
10 **flies store and dynamically update memories of the direction to return them to the plume's boundary.**
11 **Consistent with this, we find that FC2 neurons within the fan-shaped body, which encode a fly's**
12 **navigational goal, signal the direction back to the odor boundary when flies are outside the plume.**
13 **Together, our studies suggest that flies leverage the plume's boundary as a dynamic landmark to guide**
14 **their navigation, analogous to the memory-based strategies other insects use for long-distance**
15 **migration or homing to their nests. Plume tracking thus uses components of a conserved navigational**
16 **toolkit, enabling flies to use memory mechanisms to navigate through a complex shifting chemical**
17 **landscape.**

18 Navigating within a complex environment is a ubiquitous requirement for all animals, driving the evolution
19 of diverse behavioral strategies tailored to the structure and stability of different sensory landscapes[1]. In
20 many instances, animals can effectively navigate using a simple chain of sensorimotor reflexes in which
21 they steer towards or away from a salient object based solely on immediate sensory cues[2,3]. However,
22 when sensory signals are intermittent or unreliable, memory mechanisms may facilitate navigation by
23 allowing animals to store the position of stable landmarks in their environment and use an allocentric
24 representation of space to track towards objects that cannot be continuously sensed. Insects, for example,
25 are thought to use a vector-based navigational strategy in which they integrate directional and distance
26 information to guide them toward a remembered location[3,4]. Such an approach is exemplified by the
27 navigational feats of central place foragers, like ants and bees, who can wander far from their nest and
28 efficiently return even in a largely featureless environment[3,5]. However, whether similar vector-based
29 strategies can be used to steer through a more dynamic sensory environment, like an odor plume wafting
30 from its source, has remained unclear[2,6,7].

Odors are among the most salient signals that insects use to guide navigation[8]. Plume tracking in insects has been proposed to rely on a largely reflexive strategy in which animals surge upwind upon encountering an odor and cast crosswind upon losing contact with the plume in order to re-encounter it[9–11]. Yet, the intrinsically dynamic nature of olfactory plumes often requires animals to navigate using only brief intermittent odor encounters[2,12], separated by vast stretches of clean air that that offer no immediate sensory information that could point them back to the plume. Memory mechanisms could allow animals to bridge across their fragmented experience of the odor, for example by enabling them to store the direction of their last odor encounter to guide their returns to the plume. We therefore asked whether *Drosophila* can track a plume using components of the same vector-based navigational strategy that central place foragers use to home to their nests. By developing a virtual reality paradigm for plume navigation, we show that *Drosophila* indeed store the heading direction required to return to the plume's boundary as a dynamic landmark, continuously updating this goal direction as they track along the plume's border. Consistent with the notion that a plume is not associated with a fixed point in space, flies appear to retain a memory only indicating the direction to the plume's boundary, not their distance from it. Our results suggest how elements of a conserved navigational toolkit[13] can be flexibly deployed in different sensory contexts, allowing flies to use odors as remembered chemical signposts to track long distances towards a remote source.

Flies track a plume along its boundary

One fundamental challenge to elucidating the behavioral algorithms underlying plume navigation is that odors are invisible and often carried along turbulent fluid flow[2,14]. Consequently, few experimental systems offer access to an animal's true sensory experience as it navigates an odor plume, or to the underlying neural dynamics used to guide behavior. To overcome this limitation, we developed a closed-loop olfactory paradigm that allows head-fixed *Drosophila* to navigate virtual chemical landscapes. In this system, the heading of a tethered fly walking on an air-supported ball is yoked to the rotation of a tube carrying a constant airstream, enabling the fly to control its orientation relative to a wind source blowing from a constant direction in an external or allocentric reference frame[15,16] (**Fig. 1a, Supplementary Video 1**). By coupling two high-speed mass flow controllers to the virtual XY position of the fly, we could dynamically control the concentration of odor infused into the airstream at each moment as the fly explored this two-dimensional virtual world, allowing us to construct plumes of almost any spatial structure. Notably, in this paradigm flies walk in complete darkness and thus can only navigate using spatial information conveyed by the direction of the wind source and, when they are in the plume, the identity and concentration of the odor. This virtual paradigm thus offers precise control of a fly's sensory environment, allowing us to investigate how navigational strategies are shaped by ongoing or past odor encounters.

We reasoned that memory mechanisms to facilitate navigation might be most apparent in the context of a stationary plume which, through its stability, would allow flies to accumulate useful information about its structure. We therefore initially explored how flies navigate a 50 mm fictive 'corridor' of the appetitive food odor apple cider vinegar oriented parallel to the wind direction (ACV, **Fig. 1b**)—a highly simplified chemical landscape that nevertheless recapitulates several key features of the slowly dispersing surface plumes that walking flies encounter in nature when close to their source[12]. The odor corridor was bounded

72   on both sides, such that if a fly walked laterally (crosswind) too far in one direction or the other, it would
73   exit the boundaries of the fictive plume and the ACV concentration would decrease rapidly (**Fig. 1a,b**)).
74   Due to the finite time required for odor entering the airstream to reach the fly's antenna (~500 ms), the
75   lateral boundaries of the fictive plume were not perfectly sharp but decayed within ~5 mm, depending on
76   the walking speed of the fly (**Extended Data Fig. 1b**). A shallower gradient ran along the longitudinal
77   direction of the corridor, such that a fly would experience a steadily increasing concentration of ACV (10-
78   100% over 1 meter) as it walked upwind, mimicking the sensory feedback of getting closer to the odor
79   source.
80
81   Prior descriptions of plume tracking suggest that flies may navigate this corridor through odor-gated
82   anemotaxis, reorienting and surging upwind upon contacting the odor corridor, while remaining largely
83   confined within its boundaries[1,9–11,17,18]. However, we found that tethered flies reliably ascended the
84   entire length of the plume by tracking along a single edge through the repeated implementation of two
85   behavioral motifs: upon entering the corridor, they rapidly counter-turned to exit it, and once outside the
86   plume they performed a more circuitous exploration before re-entering (**Fig. 1b, Supplementary Video
87   2**). We call this behavior 'edge tracking'.
88
89   During edge tracking, flies traveled inside the plume briefly, spending only around 2.01 sec (mean, 95%
90   confidence interval: 1.91 to 2.15 sec, n=755 bouts) in odor before exiting the plume's boundaries (**Fig. 1c**).
91   As a consequence, animals spent significantly more time outside the odor corridor than inside of it as they
92   ascended upwind along the plume's boundary. Nevertheless, most of their progress towards the fictive
93   odor source occurred during these brief inside bouts (**Fig. 1b,d**) as flies accelerated upwind upon entering
94   the odor, prior to counter-turning and leaving it. On average, flies also progressed upwind when they
95   walked outside the plume (**Fig. 1b,d**), but these outside trajectories were far more variable in both
96   distance and duration, with some excursions extending hundreds of millimeters orthogonal to the plume's
97   boundary before returning (**Fig. 1c,d**). Flies typically tracked along a single edge, spending most of their
98   time within the lateral 4.65 mm margin (mean, 95% confidence interval, 4.54 to 5.14 mm) of the odor
99   corridor and rarely crossing the plume's width to the other edge. Indeed, >96% of the time flies entered
100   the plume, they exited along the same edge (n=793 inside bouts, n= 40 flies). The majority of flies initially
101   encountering an ACV corridor spontaneously tracked its edge for hundreds of millimeters (**Extended Data
102   Fig. 2**), underscoring that edge tracking represents a robust strategy to navigate spatially structured
103   chemical landscapes.
104
105   Animals can use perceived changes in odor concentration, sampled either spatially or over time, to localize
106   an odor source[1]. To assess whether edge-tracking flies relied on the increasing odor concentration
107   experienced as they ascended the plume, we provided them with a corridor of the same dimensions but
108   with a constant odor concentration (20% ACV). Individual flies tracked this constant concentration
109   corridor as effectively as plumes in which a longitudinal gradient was present (**Extended Data Fig. 3a,b**),
110   indicating that feedback about increasing odor intensity was not necessary to sustain continued pursuit
111   towards the fictive odor source. Indeed, flies even tracked the edge of a corridor in which the odor
112   gradient was reversed such that as animals progressed upwind, they encountered successively lower
113   concentrations of ACV (**Extended Data Fig. 3a**), a configuration rarely encountered in nature. On average,

114   the trajectories of flies were indistinguishable whether they tracked plumes of constant, increasing or
115   decreasing odor concentration (**Extended Data Fig. 3b**). Flies in our paradigm thus appear sensitive to the
116   presence of odor but not its instantaneous concentration. These observations align with the notion that
117   in naturalistic plumes the intermittent packets of odor that a fly may encounter rarely contain
118   concentration gradients that point to the odor source or can be used to guide navigation[14,19,20]. Flies in
119   our paradigm thus do not appear to rely on the gradual changes in odor concentration along the plume's
120   longitudinal axis to maintain pursuit. Rather the lateral boundaries of the plume, the region of highest
121   contrast between odor and no odor, may represent a key sensory feature that guides plume tracking.
122
123   Edge tracking is reminiscent of descriptions of insects and other arthropods that track the boundary of a
124   surface plume using bilateral comparisons of their chemosensory appendages[21–27]. However, the
125   boundaries of our fictive plume arise from rapid temporal changes in odor concentration that are nearly
126   synchronous between the left and right antenna (**Extended Data Fig. 4a**). To assess whether flies use
127   transient asymmetries in the sensory signals to their two antennae, we expressed the optogenetic
128   activator CsChrimson in the majority of olfactory sensory neurons using the *Orco* promoter, allowing for
129   simultaneous activation of both antennae as flies weaved in and out of a 660 nm light corridor (**Extended
130   Data Fig. 4b**). In the absence of wind, Orco>CsChrimson flies preferentially remained within the light
131   corridor (**Extended Data Fig. 4c,d**), consistent with the intrinsically appetitive nature of broad olfactory
132   sensory neuron activation[22,28,29]. However, these flies progressed minimally in either direction along the
133   plume's longitudinal axis (**Extended Data Fig. 4e**), further underscoring that the wind provides a critical
134   directional cue to propel animals along the boundary. Indeed, when we added a closed-loop wind source,
135   Orco>CsChrimson flies ascended upwind, adhering to the boundary of the fictive odor plume using a
136   similar behavioral strategy as observed during edge tracking of an ACV corridor (**Extended Data Fig. 4c,d**).
137   Flies thus do not appear to require a bilateral comparison of olfactory input to localize the plume's edge
138   but rather rely on wind direction and the steep change in odor concentration at the lateral boundary as
139   spatial cues to edge track.
140
141   **Edge tracking is not a random search process**
142   In our setup, once a fly is outside the plume, the wind is the only sensory signal that can be used as a
143   directional reference, which in our virtual paradigm blows from a constant allocentric direction. While
144   many flies in our experiments closely adhered to the plume's edge, with only transient outside excursions,
145   some occasionally performed long trajectories that placed them hundreds of millimeters away from the
146   plume's boundary (**Fig. 1c**). During these distant excursions, flies were immersed in clean air for tens of
147   seconds before returning back to the edge, frequently through a shorter more-directed path (**Fig. 1c-e**),
148   suggesting that they may retain information about the direction or location of the plume to guide their
149   returns. To examine the structure of a fly's exploration outside the odor corridor, we divided each outside
150   trajectory into an 'outbound' and 'inbound' segment based on the most distant point from the plume's
151   boundary. Flies typically exited and returned to the plume's edge using distinct routes. During outbound
152   trajectories, flies left the plume at a shallow angle relative to the plume's edge, steering strongly upwind.
153   In contrast, inbound trajectories were often angled almost perpendicular to the plume's edge and
154   followed shorter paths such that, on average, flies took more direct paths back to the odor corridor (**Fig.

155   **1f).** Calculating the average path of all the trajectories for an individual fly further supported the
156   asymmetry of their routes away from and back to the plume's edge (**Fig. 1e**).

157

158   The observation that animals take lengthy excursions away from the plume and make directed returns
159   back to its boundary suggests that their outside exploration may not be random. To gain further insight
160   into the structure of a fly's trajectories outside the plume, we decomposed them into their elementary
161   run lengths and turn angles (**Extended Data Fig. 5a,b** Methods), then randomly drew from these
162   experimental distributions to generate synthetic trajectories built from the same path statistics but
163   lacking any directional biases, analogous to the reflexive and random casting that insects have been
164   proposed to perform when they lose contact with a plume[1,30]. Simulated trajectories could reliably return
165   to the plume's boundary (**Fig. 1g**) but displayed several differences from the trajectories of real edge-
166   tracking flies. Notably, while simulated trajectories could extend far away from the plume, they were
167   highly circuitous and took significantly longer overall path lengths to return. For example, in our dataset,
168   flies walked up to 320 mm from the lateral boundary of the plume, taking a total roundtrip path of 1.5
169   m—a distance just over twice the length of the most efficient path they could achieve by walking directly
170   away from the plume and directly back. Simulations of similarly lengthy outside excursions, by contrast,
171   took ~15 times longer than the most efficient paths (**Fig. 1g**). Additionally, while the outside trajectories
172   of real flies were significantly shorter on the inbound than outbound segments, reflecting more directed
173   returns, the outbound and inbound segments of simulated trajectories were equivalent in length,
174   consistent with their undirected nature (**Extended Data Fig. 5d**). Finally, real flies display an intrinsic
175   upwind bias[16,31,32] and continued to walk upwind even outside the plume. Adding the experimentally
176   observed upwind bias (**Extended Data Fig. 5c**) resulted in simulated trajectories that ascended the plume
177   like those of real flies. However, this upwind bias had no impact on the efficiency of simulated trajectories
178   (**Fig. 1g, Extended Data Fig. 5c,e**), consistent with the fact that the most efficient path to return to a
179   vertically-oriented odor corridor depends only on the ability to progress in the crosswind, not upwind,
180   direction. Edge tracking therefore does not adhere to the statistics of a random search process. Rather,
181   the directed returns to the plume's edge observed in edge-tracking flies suggest they rely on a memory
182   of past plume encounters to guide efficient trajectories back to the boundary.

183

184   **Flies can track plumes with different geometries**
185   The nature of memory mechanisms that facilitate navigation back to the plume could take several forms,
186   from simply biasing the direction of an animal's search, as observed after a hungry fly consumes a sugar
187   droplet[33,34], to storing the specific location of the plume's boundary and homing towards it via path
188   integration, as displayed in foraging ants returning to their nest[5,35]. To shed light on the algorithms that
189   flies may use for edge tracking, we leveraged the virtual nature of our paradigm to vary the structure of
190   the fictive chemical landscape, by changing either the orientation and stability of the plume or modifying
191   the fly's distance to it.

192

193   Transient shifts in wind direction may cause a plume to meander, such that it no longer aligns with the
194   wind direction or points to the odor source. Employing a reflexive behavioral strategy in which an animal
195   surges upwind upon encountering the odor would inevitably cause it to walk out of a meandering plume,
196   leading to the proposal that it may be advantageous to track the envelope of the plume rather than the

197   wind direction[36]. To explore this possibility, we constructed a set of 'tilted' plumes of constant ACV
198   concentration, in which the longitudinal axis of the 50 mm corridor was offset from the wind direction by
199   either 45 or 90 degrees (**Fig. 2a-c**). We found that flies robustly tracked the boundaries of these tilted
200   plumes for many hundreds of millimeters, even for the 90-degree plume which required flies to initially
201   choose a left or right crosswind direction and progress along it, moving orthogonal to the wind with
202   minimal backtracking. Indeed, flies even tracked the edge of a 90-degree plume along a diminishing
203   concentration gradient (**Extended Data Fig. 3c,d**), reinforcing that their progression does not depend on
204   the instantaneous odor concentration. Rather flies appear to use an internal sense of direction allowing
205   them to advance in a given direction for hundreds of millimeters.

206

207   Flies tracked the boundaries of both 45- and 90-degree tilted plumes along their upwind edge using a
208   similar behavioral strategy as the vertically oriented plume (0-degree): upon entering the odor corridor,
209   they rapidly reoriented to steer upwind, and upon losing contact with the plume, they performed directed
210   returns back to the plume's boundary (**Fig. 2e-g, Extended Data Fig. 6a,c-e**). However, flies adopted
211   distinct angles to enter and exit a plume that depended on its geometry. For example, to exit a vertical
212   odor corridor while maintaining an upwind bias requires that animals steer laterally away from the upwind
213   direction to counterturn out. By contrast, flies could leave the 45- and 90-degree plume using a large
214   range of upwind angles, including directly upwind. Yet, on average individuals did not use the full range
215   of possible exit angles that could maintain an upwind bias, but rather adopted a relatively narrow range
216   of exit angles that were frequently biased in the direction that they were progressing along the plume's
217   length (**Fig. 2e-g, Extended Data Fig. 6a,c-e**). Likewise, entry angles also depended on the plume's
218   orientation, reflecting the fact that returning to a vertical plume requires animals to walk in a crosswind
219   direction, but returning to a 90° plume requires them to direct their trajectories downwind. Inside
220   trajectories were shorter in tilted plumes compared to vertical plumes (**Extended Data Fig. 6b**), as flies
221   exited more rapidly when steering upwind within the odor. In contrast, trajectories outside of tilted
222   plumes were on average the same length even when flies had to counter their intrinsic upwind drive[16,31,32]
223   outside the plume to return back to its boundary (**Extended Data Fig. 6b**).

224

225   Comparing simulated trajectories—generated by randomly selecting from the experimental distribution
226   of run lengths and turn angles—with the paths of real flies underscored the importance of these biases to
227   effectively track a tilted plume (**Extended Data Fig. 5f-g**). As observed for a vertical plume, simulated
228   trajectories that lacked an upwind bias were frequently able to return to the boundary of a 45- or 90-
229   degree plume, although far less efficiently than real trajectories. However, incorporating the inherent
230   upwind bias displayed by real flies as they walk outside the plume (**Fig. 1b,d**) resulted in simulated
231   trajectories that strayed far away from the boundary and often failed to return (**Extended Data Fig. 5f-g**),
232   emphasizing that successfully tracking a tilted plume requires flies to counter their upwind drive to
233   reenter. Flies thus appear to adapt their trajectories to the geometry of the plume. Even in clean air,
234   where flies have nothing but the wind direction to serve as a navigational cue, they adopt different biases
235   to return to the plume depending on its geometry—directing their trajectories crosswind to return to a 0-
236   degree plume but steering downwind to return to a 90-degree plume (**Fig. 2e-g, Extended Data Fig. 6c-**
237   **e)**.

238

239   To determine whether flies rely on a memory of the direction of the plume's boundary to guide their
240   returns, we allowed flies to track the edge of a vertical, 45- or 90- degree plume for 10 minutes before
241   removing the plume while they were on an outside excursion (**Fig. 2i**). We found that after the plume's
242   disappearance, flies continued to walk in the same direction that they had previously used to return to
243   the plume and maintained this distinct directional bias for tens of seconds, even though this often took
244   them hundreds of millimeters away from the location of their last plume encounter. The directional biases
245   differed across the three plume geometries and were distinct from the upwind bias that flies generally
246   displayed in the two minutes prior to encountering the plume (**Fig. 2i,j**), even though they had continuous
247   access to the same closed-loop wind source to orient them. Thus flies appear to form and maintain a
248   persistent directional bias that depends on the orientation of the plume that they had been previously
249   tracking. While the disappearance of a sugar droplet has been shown to trigger flies to perform a local
250   search centered around the previously encountered reward location[34], flies did not dwell around the
251   location of their last plume encounters, suggesting that edge tracking does not involve positional
252   information.

254   One implication of storing a directional bias back to the edge is that it should allow flies to effectively track
255   dynamic plumes, even as they shift over time. To explore this possibility, we jumped the position of the
256   plume each time a fly exited it by moving the boundary 20 mm in the direction opposite to their exit (**Fig.
257   2d,h**). Successful navigation of this dynamic plume requires flies to not only bias their return trajectory in
258   the direction of the plume's boundary, but to walk even further in this direction to re-encounter it,
259   resulting in significantly longer trajectories than for stationary plumes (**Extended Data Fig. 6b**). Flies
260   readily returned to and tracked the jumping plume (**Extended Data Fig. 5h, Supplementary Video 3**),
261   consistent with the persistent directional bias they displayed when the plume disappeared, allowing them
262   to return to a plume even as it meandered away from the last encountered position. Notably, flies did
263   not search for the plume boundary at its pre-shifted location, providing further support for directional but
264   not positional memory.

Edge tracking requires the fly compass system
267   Our behavioral analyses suggest that flies rely on a directional memory of the plume's boundary to bias
268   their outside trajectories and direct their returns. We reasoned that the central complex, an array of
269   evolutionarily conserved neuropils underlying spatial navigation in insects[3], might serve as an ideal neural
270   substrate for encoding and storing memories of the plume's direction that could be used to guide edge
271   tracking. A core spatial signal encoded in the *Drosophila* central complex is a fly's heading direction, which
272   is represented as a single bolus of activity that rotates around topographically organized EPG neurons in
273   the ellipsoid body[37]. This neural compass can be anchored to stationary visual landmarks, such as the
274   sun[38–40] or mechanosensory landmarks such as a wind source[41] to allow animals to maintain a stable
275   heading as they fly or walk in a fixed direction[32,39,42,43]. Edge-tracking flies navigate in complete darkness,
276   leaving the wind direction as the sole external landmark available to orient themselves as they weave in
277   and out of the plume.

279   Ascending pathways conveying information about wind direction are thought to entrain the activity of
280   EPG neurons[41], allowing flies to use a stable wind source to maintain an accurate allocentric

281 representation of their heading in the world. To examine the activity of EPG neurons during edge tracking,
282 we performed two-photon functional calcium imaging of their axon terminals within the protocerebral
283 bridge, a linear neuropil comprised of 18 glomeruli that receives two duplicated copies of an animal's
284 heading direction (**Fig. 3a**). Consistent with prior recordings of EPG neurons during visual navigation tasks,
285 we observed two discrete boluses of neural activity that moved in concert across the left and right halves
286 of the protocerebral bridge, with their position locked to the fly's heading direction relative to the wind
287 (the EPG 'phase'). In flies walking in the absence of external visual landmarks that can be used for
288 corrective feedback, the EPG phase can rapidly drift relative to the animal's true behavioral
289 heading[37,44,45]. However, during edge tracking, the EPG phase remained faithfully aligned to the fly's
290 heading direction in the virtual environment over the course of tens of minutes (**Fig. 3b,c**), underscoring
291 their ability to use a wind source as a stable landmark[41]. The amplitude and width of the boluses of EPG
292 activity in the protocerebral bridge were comparable throughout the course of an edge-tracking trial,
293 indicating that this heading signal remains yoked to the wind and unchanged by the presence of odor (**Fig.**
294 **3d**).

295

296 The representation of an animal's current heading by EPG neurons is thought to be integral to *Drosophila*
297 navigation as this signal may be transformed and reformatted to generate other spatial variables, such as
298 an animal's traveling direction[46,47] or compared to an animal's stored goal direction to guide its moment-
299 to-moment steering behavior[32,43,48–50]. To assess whether edge tracking relies on this core navigational
300 signal, we used an intersectional genetic driver to express the light-gated anion channel GtACR1 in EPG
301 neurons and acutely inhibit their activity during edge tracking. We focused on flies tracking a jumping
302 plume given that successful navigation requires animals to maintain a persistent bias to return to the
303 plume's shifted edge (**Fig. 2d,h**) and may thus reveal the need for a continuous representation of an
304 animal's heading. Indeed, upon silencing of EPG neurons, flies no longer made directed returns to the
305 plume's shifted boundary but instead frequently wandered away in the upwind direction (**Fig. 3e**).
306 Consequently, in trials in which EPG neurons were inhibited, flies made fewer returns to the plume's
307 boundary (**Fig. 3f**). When they did manage to return, they took longer, often entering the plume hundreds
308 of millimeters farther upwind in contrast to the directed, crosswind returns observed in control flies (**Fig.**
309 **3e,f**). No differences in the frequency of returns or upwind entry position were apparent in control
310 animals (UAS-GtACR1), independent of whether the optogenetic stimulating LED was on or off, supporting
311 the specificity of this manipulation. EPG neuron activity thus appears to be required for edge tracking.
312 Navigation of structured chemical landscapes therefore appears to represent a spatial navigation task that
313 depends on core elements of the central complex circuitry.

314

315 **Flies rely on odor entry and exit angles to guide plume navigation**
316 What spatial cues might flies use to form or update a memory of the plume's direction during edge
317 tracking? While flies could in theory enter or exit an odor corridor over a 180-degree range, they
318 consistently adopted a narrower range of angles that depended on the plume's geometry (**Fig. 2e-h,**
319 **Extended Data Fig. 6c-f**). We therefore hypothesized that each time a fly crossed the edge of the plume,
320 it used the angle of its current heading relative to the wind direction to form an angular memory that
321 could guide subsequent trajectories. If so, odor encounters uncoupled from their corresponding entry or
322 exit angles should lead to different trajectories outside the plume. To investigate this possibility, we

323   allowed a fly to track the boundary of an odor corridor for 10 minutes and then immediately replayed the
324   identical temporal sequence of odor pulses back to the same individual or to a naive animal that had never
325   edge tracked (**Fig. 4a**). During these 'replay' epochs, the wind source remained unchanged and yoked to
326   the fly's angular heading, but the fly's odor experience was now completely uncoupled from its actions
327   and, in particular, from the angle that the fly was traveling at the time of odor onset or offset.

328

329   We focused on flies tracking along the boundary of a 90-degree plume given that this requires animals to
330   bias their outside trajectories downwind to reenter the plume, which allowed us to uncouple the biases
331   in an animal's trajectories arising from its intrinsic upwind drive[16,32] from those emerging from their recent
332   edge-tracking experience. During the replay epoch, we found that flies that had previously tracked along
333   a 90° plume initially continued to display the same directional biases that they had used to return to the
334   odor corridor: upon odor onset they steered in the upwind direction, while at odor offset they
335   counterturned to travel in a downwind direction (**Fig. 4**). However, this downwind bias rapidly decayed
336   with subsequent encounters, and the traveling direction of flies during replay progressively shifted
337   towards the upwind direction (**Fig. 4c**). In contrast, naive flies presented with the same temporal
338   sequence of odor pulses surged upwind at odor onset and continued to travel in an upwind direction after
339   odor offset, giving rise to trajectories with a net upwind bias (**Fig. 4a,** right). Thus while naive flies track
340   upwind, analogous to prior reflexive descriptions of plume tracking[9,17,18], individuals that had recently
341   tracked the edge of a 90-degree plume maintained a directional bias based on their past plume
342   encounters that gradually eroded. Together, these results suggest that the paths that flies take as they
343   weave in and out of an odor plume depend on the spatial structure of their previous odor encounters,
344   such that even identical temporal patterns of odor stimulation can give rise to distinct trajectories
345   depending on the fly's orientation at the time of odor onset or offset. Based on these observations, we
346   conclude that edge tracking flies use their recent entry and exit angles to form and update their goal
347   direction, allowing them to navigate away from and back to the plume's boundary.

348

349   **A behavioral model of edge tracking**
350   To gain further insight into how flies use their past plume encounters to shape their navigational goals,
351   we developed a switching state space model[51,52] in which simulated animals alternate between 'leaving'
352   and 'returning' states as they progress along a plume's boundary (**Fig. 5a**). These states do not correspond
353   directly to the epochs when the fly is inside or outside the plume, although the transition rates between
354   them depend on the presence or absence of odor **(Extended Data Fig. 7a,b)**. This model generates a
355   velocity vector for the simulated fly through an auto-regressive process, with a correlation timescale and
356   noise level determined by the current state. Importantly, the velocity vector is biased by a memory of
357   previous exit angles (for the leaving state) or previous entry angles (for the returning state). These
358   memories are updated each time the fly crosses the odor boundary by replacing the current memory with
359   a linear combination of that memory and the direction of motion at the time of the odor crossing. As a
360   consequence, flies in our model rely on entry angles over multiple odor encounters to form and update a
361   goal direction that biases their velocities in the returning state, while they use their exit angles to form
362   and update a goal direction that similarly biases their leaving state. We used variational inference to
363   extract the latent leaving and returning states, and latent goal directions, and to learn the parameters
364   determining the velocity and memory updates from the trajectories of individual flies tracking different

365   plume geometries (**Extended Data Fig. 7g, Model Methods**). Model parameters varied across flies,
366   matching the heterogeneity that flies display in their outside trajectories, with some individuals adhering
367   closely to the plume's boundary and others taking longer and more circuitous excursions before returning
368   (**Extended Data Fig. 7c-f**). From these fits, we computed average model parameters to simulate fly
369   trajectories and reveal how leaving and returning goal directions emerge from repeated plume
370   encounters (**Fig. 5b**).
371
372   The model requires that we initialize the memory vectors at the beginning of a simulation. In the absence
373   of information about the prior olfactory experience of a given fly, we set the initial exit memory to be
374   upwind with a narrow randomly chosen crosswind component (see Model Methods), in accord with the
375   observed upwind bias that flies display as they exit all plumes (**Fig. 2e-h, Extended Data Fig. 6c-f**). The
376   memory of the entry angle, on the other hand, was initialized as a null vector, consistent with the
377   assumption that flies have no prior information about which direction to return before encountering a
378   plume. Simulations based on this model capture the ability of flies to track the edges of plumes with
379   different geometries and match the statistics of their experimental trajectories (**Fig. 5b-d**, **Extended Data**
380   **Fig. 8**). Simulated trajectories from a model lacking an entry angle memory were significantly less effective
381   in advancing along the plume's boundary for all plume orientations (**Extended Data Fig. 9a,e**). Likewise,
382   simulations using an exit memory that was either purely upwind or contained a crosswind component
383   that was resampled with each exit were also impaired in some plume geometries (**Extended Data Fig. 9c-**
384   **e**). In contrast, a model in which the exit angle memory maintained a constant crosswind bias could edge
385   track successfully (**Extended Data Fig. 9b,e**). These results align with evidence that flies strongly bias their
386   entry angles to track plumes of different orientations (**Fig. 2e-h, Extended Data Fig. 6c-f**). By contrast, flies
387   exhibit less variation in their exit angles, which display a small consistent crosswind bias that is only
388   minimally influenced by a fly's subsequent edge-tracking experience (**Extended Data Fig. 9f-g**).
389
390   Our model provides insight about the timescales of memory formation and updating that shape edge
391   tracking behavior. For instance, the model posits that flies have no initial entry angle memory, but a goal
392   is established and reinforced with repeated plume encounters as an animal repeatedly enters the odor
393   corridor at consistent angles. Indeed, both real and simulated outside trajectories become more efficient
394   over time (**Extended Data Fig. 10a**). This effect was only significant for the 90° and jumping plumes, likely
395   because these configurations cause flies to be displaced further from the plume's edge. Once an exit or
396   entry angle memory is formed, the model predicts that it will be retained in the absence of additional
397   experience, in accord with our observation that animals continue to travel for tens of seconds in the
398   direction of a previously encountered plume that has suddenly vanished (**Fig. 2i**). On the other hand,
399   simulation of the olfactory replay experiments suggest that an animal's entry angle memory can be rapidly
400   updated through a small number of additional odor encounters (**Fig. 4d, Extended Data Fig. 9f, Extended**
401   **Data Fig. 10b,c**), allowing animals to flexibly adapt their navigational goals.
402
403   To explore the timescales of memory updating, we provided flies with a plume consisting of two 45-degree
404   segments oriented in opposite directions relative to the wind (±45°) and examined how a given entry
405   angle memory adapts due to additional odor encounters in a different direction (**Fig. 5e, Extended Data**
406   **Fig. 11a**). Successfully tracking both segments requires distinct entry angle memories that are

10

407   approximately 90 degrees apart. After tracking the first (+45°) plume segment, the majority of flies

408   continued to travel away from the plume, replicating the persistent directional bias observed when the

409   plume disappeared (**Fig. 2i, Extended Data Fig. 11c**). As a consequence, flies rarely re-encountered the

410   second (-45°) segment or succeeded in tracking upwind along its boundary (**Fig. 5h, Extended Data Fig.**

411   **11b,d**), consistent with the notion that they require additional olfactory experience to update their goal

412   direction.

413

414   We therefore introduced an operant 'training' session after animals tracked the first +45° plume segment

415   to update the entry angle memory by exposing a fly to odor when it spontaneously walked in the direction

416   required to enter the second segment's boundary (e.g. -90° to -135°, **Fig. 5e**, **Extended Data Fig.**

417   **11a**). Model simulations indicated that the entry angle memory could be shifted to a new angle by a small

418   number of successive odor encounters at that angle (**Fig. 5g, Extended Data Fig. 9g**). Indeed, flies trained

419   with a single operant session were significantly more successful in tracking the second plume segment

420   than flies without this training, suggesting they incorporated a modified entry angle memory (**Fig.**

421   **5f**). Additional operant training sessions in the same direction (5 sequential bouts) provided no further

422   enhancement, whereas flies trained in the opposite direction, by exposing them to odor if they walked in

423   the direction that matched their reentry into the first plume segment (+90° to +135°), performed similarly

424   to untrained flies (**Extended Data Fig. 11b,d**). Together, these experiments support the idea that flies bias

425   their return to the plume's boundary using an angular memory that can be updated dynamically as the

426   orientation of the plume shifts, allowing for flexible navigation in a shifting chemical environment.

427

428   **Dynamic goal signals within the central complex**

429   Our behavioral model has two dynamic components: stochastic transitions between leaving and returning

430   states that depend on the presence or absence of odor, and state-dependent updates of velocity and

431   memory vectors (**Extended Data Fig. 6a**). While we do not attempt to assign the state-determining

432   component of the model to any specific circuitry of the fly brain, its velocity and memory vector

433   representations map well onto the circuitry of the fan-shaped body in the *Drosophila* central complex (**Fig.**

434   **6a**). In particular, the fan-shaped body is thought to encode allocentric goal signals that could guide

435   olfactory navigation through its grid-like organization of intersecting columnar and tangential neurons.

436   Columnar neurons of the fan-shaped body integrate wind and heading signals to represent spatial

437   variables[46,47,53,54], such as a fly's traveling direction, as vectors through sinusoidal population activity.

438   Tangential neurons receive input from olfactory pathways[49,55,56] and are thus poised to modulate the

439   vector representations of columnar neurons during plume tracking. Based on this suggestive circuit

440   architecture, we hypothesize that the memory of a fly's entry direction, as it weaves into and out of the

441   plume, is stored as a sinusoidal pattern in the strengths of plastic synapses between tangential and

442   columnar neurons, analogous to other anatomically-inspired models of angular goal formation in

443   *Drosophila*[48,50]. Memory updates could be driven by tangential neurons that are activated at the time of

444   plume boundary crossings[55]. Distinct odor-responsive tangential neurons could gate the use of these exit

445   and entry angle memories, allowing animals to recall different goal directions when they are in the leaving

446   and returning states. The resulting goal direction is then compared to the fly's current heading to generate

447   corrective steering signals that guide the moment-to-moment motor patterns of navigation[32,43,48,49].

448

449   To gain functional evidence supporting this model, we examined the activity of FC2 neurons. This
450   columnar population encodes a fly's goal as a stable bolus of activity during bouts of menotaxis[32], in which
451   a fly walks in a consistent direction relative to a visual landmark, keeping its goal and heading aligned.
452   Moreover, FC2 neurons directly synapse onto PFL3 neurons, an output pathway of the central complex
453   that controls steering by comparing an animal's current heading with its goal[32,43,48,49]. FC2 neurons receive
454   input from multiple tangential and columnar populations[49], positioning them to encode distinct goal
455   signals in different behavioral states or contexts. However, whether FC2 neuron activity flexibly
456   represents an animal's changing goals has not been explored.

458   To assess whether FC2 neurons reflect a fly's leaving goal, returning goal or alternate between both, we
459   simultaneously recorded the activity of EPG and FC2 neurons as animals walked in clean air and then
460   initiated edge tracking along an odor corridor. The elevated temperatures associated with two-photon
461   imaging can induce dispersal behavior[32,39,47], promoting straight trajectories with a strong upwind bias,
462   which significantly reduces the crosswind distance animals walk away from the plume's edge. Therefore,
463   to encourage flies to rely on their memory of the direction toward the plume, we used the jumping plume
464   in which we periodically shifted the plume's boundary while flies were on an outside trajectory (**Fig. 6b**).
465   This requires flies to walk further on their return paths (**Extended Data Fig. 6b**), preventing them from
466   incidentally re-encountering the plume's boundary.

468   Prior to edge tracking, as flies walked upwind in clean air, we observed that the phases of EPG and FC2
469   neurons remained largely aligned (**Fig. 6d,e**), matching their relationship during menotaxis[32]. During edge
470   tracking, however, the phase of FC2 neurons frequently diverged from the EPG signal (**Fig. 6c**). Notably,
471   the FC2 phase tracked a fly's current heading inside the odor and as it initially exited the plume, but began
472   to point back in the direction of the plume several seconds before the animal turned towards it on return
473   trajectories (**Fig. 6c,f-j**). The lag between the emergence of this FC2 signal and the subsequent steering of
474   the fly towards the plume (**Fig. 6j**) resembles the time course of the corrective steering flies display when
475   an arbitrary goal angle is experimentally imposed on this columnar population using targeted
476   optogenetics[32]. FC2 neurons thus appear to selectively signal a memory-dependent goal of the entry angle
477   that could guide their returns to the plume's boundary.

479   **Discussion**
480   Odors serve as essential navigational cues for many species despite carrying no inherent directional
481   information. Animals must therefore integrate chemical cues with spatial signals to track an odor to its
482   source, a necessity thought to act as a potent force shaping the evolution of navigational circuits[57,58].
483   Indeed, the close evolutionary relationship of ancestral forebrain circuits, such as the piriform and
484   entorhinal cortex in mammals[59,60,61], and the extensive connectivity between the mushroom body and
485   central complex in insects[49,55,62] exemplify how diverse species have evolved the ability to store memories
486   of their odor experience and bind these to internal representations of space.

488   In this study, we explored how insects rely on memory mechanisms to navigate a chemical landscape. By
489   developing methods to gain precise experimental control over a fly's olfactory experience, we show that
490   flies leave the plume and return to its edge repeatedly for meters. While this strategy is reminiscent of

12

491 prior descriptions that insects can track a surface plume by "feeling for its edge"[17], by experimentally
492 defining and manipulating the location of the plume's boundary, we revealed that it is in fact stored as a
493 remembered olfactory landmark. Our analyses suggest a model for how the plume's edge is endowed
494 with salience: each time a fly enters or exits the odor corridor, it dynamically updates and stores a memory
495 of its current heading direction relative to the wind. During edge tracking, flies alternately rely on the
496 integrated memory of their exit and entry angles to guide their trajectories away from the plume and back
497 to its boundary. Consistent with this, we find that FC2 neurons, which have been shown to encode a fly's
498 allocentric goal[32], signal the direction of the plume's boundary during returns.

499

500 Flies thus appear to navigate structured chemical landscapes using a vector-based strategy similar to what
501 central place foragers, like ants and bees, use to home to their nests[3,5]. However, unlike a fixed nest
502 location, the boundary of an odor plume is not stationary. Consequently, edge-tracking flies need only
503 store the relative direction to the plume's boundary rather than its specific position, simplifying memory
504 requirements. Consistent with this, flies do not revisit the site at which they exited the plume but rather
505 bias their trajectories in the direction of the plume's boundary, as they continue to advance along its
506 length. While the wind serves as an obvious directional cue that flies could use to progress up a vertically
507 oriented plume, we find that flies make similar progress along plumes oriented orthogonal to the wind,
508 by using consistent entry and exit angles that propel them in a chosen crosswind direction. These results
509 underscore that odors themselves are not the ultimate 'goal' during plume tracking but rather serve as
510 chemical signposts that an animal can use to track towards the odor's source. Edge tracking is therefore
511 reminiscent of the route following strategy ants display when navigating through dense visual
512 landscapes[63], in which they use a sequence of stored local vectors to guide them back to their nest, each
513 associated with a distinct visual snapshot along their route. Serially sampling sensory landmarks, whether
514 olfactory or visual, thus appears to be a shared component of the insect navigational toolkit[13].

515

516 For memories to have predictive value, their timescales must be aligned with the stability of the
517 environment. Once formed, the memory of the plume's edge appears to be maintained over tens of
518 seconds, as revealed by the persistent directional bias flies display once the plume vanishes. The entry
519 angle memory can nevertheless be updated rapidly over additional odor encounters, such that flies can
520 flexibly adapt to plumes oriented in different directions relative to the wind. While we focused on
521 navigation in a highly-structured chemical landscape to facilitate mapping of a directional memory to
522 plume encounters, such rapid and flexible updating suggests a similar mechanism could be relevant even
523 in the context of more turbulent plumes. The replay of an odor sequence, where a fly encounters boluses
524 of odor uncoupled from its behavior, offers insight into how vector-based navigation could shape a fly's
525 trajectories even in more chaotic sensory environments[64]. Modeling of edge tracking behavior, however,
526 indicates that memory updating is not instantaneous, but reinforced across successive odor encounters.
527 This suggests the possibility that in a turbulent plume, where odor filaments arrive from erratic directions,
528 the lack of coherence in an animal's heading direction at odor onset and offset may erode the strength of
529 any angular memory. If the spatial structure of odor encounters is truly stochastic, flies may resort to
530 more reflexive strategies or those that rely on different forms of short-term memory, such as using plume
531 intermittency to guide navigation towards the source[2,64]. Different tracking algorithms are therefore likely
532 to be engaged depending on the coherence and stability of the environment.

533 During edge tracking, flies encounter a continuous odor corridor yet, behaviorally, create a temporally
534 intermittent experience of the plume by sampling along its edge. One potential reason flies engage in
535 edge tracking is to minimize sensory adaptation[65–67]. However, flies appear relatively indifferent to the
536 concentration of odor they encounter along the longitudinal axis of the plume, suggesting sensory
537 adaptation is unlikely to be the primary driver of this behavioral strategy. Rather, we propose that the
538 plume's lateral boundary holds special significance, because as the site of the steepest concentration
539 gradient in our virtual environment, it offers maximal information about the structure of a plume[68] even
540 if it shifts. Consistent with this, artificial recurrent neural networks trained to track a shifting plume adopt
541 a plume-skimming strategy that closely mirrors edge tracking[69], demonstrating that following the
542 envelope of a plume rather than the wind direction represents a particularly robust navigational strategy.
543 Exploiting environmental contrast by following the steepest sensory gradient has been proposed to
544 underlie navigation in many biological contexts, from the paths of axonal outgrowth[70] to sonar localization
545 of bats[71], suggesting edge tracking may represent a general algorithm.
546
547 Our data suggest that edge tracking depends on the core navigational circuitry of the central complex,
548 with wind serving as an essential anchoring cue to allow flies to orient themselves in space. While our
549 switching state space model was derived only from behavioral data, it displays striking correspondence to
550 neural components within the central complex that are poised to integrate olfactory and spatial variables
551 and assign meaning to directions in space. In particular, tangential neurons within the fan-shaped body
552 responsive to odors[55] are positioned to provide modulatory signals onto columnar neurons that encode
553 spatial variables such as an animal's current heading or traveling direction[46,47,49,50] to write in the exit or
554 entry angle memory. The alternation between leaving and returning states suggests that two distinct
555 angular memories may be held in parallel and sequentially accessed as a fly weaves in and out of the
556 plume. Consistent with this, a correlate of the entry angle memory emerges in FC2 neurons as animals
557 return to the plume. Notably, we found no evidence that FC2 neurons convey signals related to the exit
558 angle, suggesting additional columnar subsets may signal the goal direction during the leaving state.
559 Alternatively, since the exit angle is predominantly in the upwind direction, an explicit memory-based
560 mechanism within the central complex may not be required. In the leaving state, odor-responsive
561 tangential neurons could suppress the activity of neurons encoding the entry angle memory, to allow flies
562 to reflexively surge upwind[9,10]. Either way, our results underscore how animals rely on dynamically
563 recruited goals to guide their trajectories as they sample along the plume's boundary.
564
565 The alternation between the leaving and returning state could tune the trajectories of an individual[5],
566 potentially giving rise to the striking variation in the efficiency of edge-tracking trajectories we observe,
567 where some animals rapidly revisit the edge, adhering closely to the plume's boundary while others take
568 more exploratory circuitous routes (**Extended Data Fig. 6d**). Tangential neurons innervating different
569 layers of the fan-shaped body integrate from distinct ensembles of lateral horn and mushroom body
570 pathways[49,55], which could allow them to dynamically regulate the strength of memory updating or the
571 timescales of the leaving and returning states depending on the innate or learned valence of an odor or
572 other contextual cues.
573

574 The central complex is thought to underlie navigation in many different insect species, from the long-
575 distance migrations of monarch butterflies to ants homing to their nest[3,5,72]. Here we reveal how flies
576 dynamically update angular memories to store direction, not distance, to a plume, exemplifying a basic
577 building block for these more complex navigational feats.
578
579 **Methods**
580 **Fly Husbandry:** Flies were maintained at 23-25°C and 60-70% relative humidity under a 12-hour light/dark
581 cycle. The quality and composition of the fly food was an important factor for eliciting robust edge-
582 tracking behavior in tethered animals, particularly during imaging experiments. We found that animals
583 raised for several generations on Wurzburg food[50] more consistently exhibited robust edge tracking than
584 those raised on standard cornmeal-agar-molasses food. All behavioral experiments were conducted using
585 starved flies which were removed from food and placed in vials containing only a water-soaked KimWipe
586 or cotton flug for 16-24 hours before tethering. For optogenetic experiments, flies were reared in
587 complete darkness. Two days prior to an experiment, 1–2-day old flies were transferred to a food vial
588 containing 0.4 mM all-trans-retinal (Sigma #R2500). 16-24 hours before an experiment flies were removed
589 from food and placed in a vial containing a Kimwipe soaked in 1-2 ml of 0.2mM all-trans-retinal in water.
590
591 **Detailed fly genotypes:**
592 For all behavioral experiments examining edge tracking of an odor plume (Fig. 1, Fig. 2, Fig. 4, Fig. 5,
593 Extended Data. 2, Extended Data. 3, Extended Data. 5, Extended Data. 7, Extended Data. 8, Extended Data.
594 9), we used:
595 • Canton-S.
596
597 For functional recording and perturbations of EPG neurons (Fig. 3), we used the SS00098 EPG split line:
598 • 19G02-p65AD ; R22E04-DBD /UAS-GCaMP7s
599 • 19G02-p65AD; R22E04-DBD /UAS-GtACR1-EYFP
600
601 For functional recording of FC2 neurons (Fig. 6) we used:
602 • VT065306-AD/UAS-syt-jGCaMP7f; VT029306-DBD /60D05-Gal4
603
604 For optogenetic activation of olfactory sensory neurons (Extended Data. 4), we used:
605 • UAS-ChrimsonmVenus/Orco-GAL4; +/+; +/+
606 • w[1118] UAS-CsChrimson.mVenus; +/+; +/+
607 Orco-GAL4, w*; +/+; +/+
608
609 *Drosophila* stock sources:
610 EPG Split Line: 19G02-p65ADZp (in attP40) ; R22E04-ZpGdbd (in attP2) Bloomington *Drosophila* Stock
611 Center (BDSC 93169); FC2 Split Line: VT065306-AD; VT029306-DBD (gift from G. Maimon); R60D05-Gal4
612 (BDSC 39247); 10XUAS-sytGCaMP7f (attP2) (BDSC 94619); 20XUAS-IVS-CsChrimson.mVenus}attP18 (BDSC
613 55134); Orco-GAL4.C}142t52.1, w[*] (BDSC 23909); UAS-GtACR1.d.EYFP}attP2 (BDSC 92983); 20XUAS-
614 IVS-jGCaMP7s}VK00005 (BDSC 79032)
615
616 **Fly tethering and dissection:** All assays were performed using 1–5-day old female flies. Flies were briefly
617 anesthetized (<10 sec) using CO_2 and tethered to a custom-milled fly-plate similar to what has been
618 previously described[73]). Flies were mounted to the fly-plate using a strand of hair or a single paint brush
619 bristle, which was used to secure their head and subsequently their body to the plate before gluing the
620 eyes and thorax using UV curable glue. In all assays, the filament was removed after successful tethering

621   and flies were placed in a dark, climate-controlled space (25 °C, 40-60% relative humidity) to recover for
622   15-30 minutes prior to the start of the experiment. Flies were then transferred to the closed loop
623   apparatus and allowed to walk freely on the ball for at least 15 minutes prior to experimentation.

625   For functional imaging experiments fly preparation varied accordingly: After tethering, the proximal
626   portion of the extended proboscis was glued to minimize movement during recording while allowing the
627   distal portion of the mouthparts to move freely during experiments. Flies were provided a recovery period
628   of 30-120 minutes after tethering. After the recovery period, the fly-plate was then filled with saline (108
629   mM NaCl, 5 mM KCl, 2 mM $CaCl_2$, 8.2 mM $MgCl_2$, 4 mM $NaHCO_3$, 1 mM NaH_2PO_4, 5 mM trehalose, 10 mM
630   sucrose, 5 mM HEPES sodium salt, pH 7.5 with osmolarity adjusted to 275 mOsm). The cuticle covering
631   the posterior portion of the brain was then cut using a 30-gauge needle and removed using forceps to
632   facilitate optical access to central complex structures. Obstructing trachea was removed taking care to
633   not damage the antenna or the antennal nerves. Flies were subsequently transferred and allowed to walk
634   on the ball for at least 15 minutes.

636   **Olfactory environment preparation:**
637   A virtual olfactory environment was created for walking tethered flies leveraging a previously described[16]
638   closed-loop olfactory system with the addition of custom python scripts that allowed for 2D odor-plume
639   rendering.

641   **Tethered locomotion**: For tethered locomotion experiments, a spherical treadmill was designed based on
642   previous studies. A 6.0 - 6.5 mm diameter ball was shaped from LAST-A-FOAM FR-4618 (General Plastics)
643   by a custom-made steel concave file. The ball rested in an aluminum base with a concave hemisphere
644   6.75 mm in diameter with a 1-mm channel drilled through the bottom and connected to an airflow. The
645   ball was recorded at 60–61 fps using a Point Grey Firefly camera (Firefly MV 0.3 MP Mono USB 2.0, Point
646   Grey, FMVU03MTM-CS) with Infinity Lens (94-mm focal length) focused on the ball, with illumination from
647   infrared LED lights. Ball rotation was calculated in real time using FicTrac software[74] running on computers
648   with ≥3-GHz processor speeds.

650   **Closed-loop arena:** The heading of the fly, as calculated by FicTrac, was transmitted to a RaspberryPi 4 via
651   serial port. Custom Python code was used to translate heading into tube position controlled by motors
652   described below. The closed-loop air delivery system was custom designed using OnShape
653   (www.onshape.com) and 3D printed using VisiJet Crystal material at XHD resolution in a 3D Systems ProJet
654   3510 HD Plus. O-ring outside dimension (OD) and inside dimension (ID) gland surfaces were designed with
655   excess material for printing and then manually modified on a lathe for improved RMS (surface) finishing.
656   360° tube rotation was driven by a bipolar stepper motor (SureStep DC integrated NEMA 17 stepper)
657   controlled through an integrated driver and coupled by a Dust-Free Timing Belt (XL Series, 1/4" width
658   (McMaster-Carr, 1679K121, trade no. 130 × L025) to the rotating tube system, which rotated mounted on
659   an Ultra-Corrosion-Resistant Stainless Steel Ball Bearing (3/4" shaft diameter, 1–5/8" OD, McMaster-Carr,
660   5908K19). The air channel was kept airtight using oil-resistant O-rings (1/16" fractional width, dash no.
661   020, McMaster-Carr, 2418T126). Motor rotation was measured by a rotary encoder (CUI Devices, AMT10
662   Series) that was used to correct for skipped steps.

664   **Airflow and Odor Delivery:** Odor delivery was achieved by directing a continuous stream of humidified
665   clean air through a 2-mm-diameter tube made of VisiJet Crystal material directed at the fly's antennae. An
666   anemometer (Kanomax 6006-DE) was used to ensure that airspeeds reaching the fly were maintained
667   between 15 and 25 cm/s. Air to the system was first passed through a charcoal filter and humidified by
668   bubbling the air through a DI water reservoir. The air flow was then split between the spherical treadmill

669   and 3 Mass Flow Controllers (MFC, Alicat, MC-Series, 1000SCCM).   Downstream of each MFC, air passed
670   through the headspace of odor vials containing either Apple Cider Vinegar (Heinz), 1-octanol or DI water.
671   The ratio of air entering each vial was dependent on the fly's position relative to the odor plume such that
672   when a fly is outside the boundaries of the plume, 100% of the air is directed into the water vial; when
673   the fly is within the boundaries of the plume, the air is directed at an experimenter-determined ratio
674   between the water vial and the odor vials. Air streams coming from the odor vials then merge with a Y-
675   connector before entering the air delivery system. Thus, by controlling how much of the air passes through
676   each vial, the MFCs control the total odor concentration of the airstream reaching the fly. The mass flow
677   controllers were controlled using a RaspberryPi 4 running custom python scripts.

678

679   **Optogenetic Stimulation:** All optogenetic experiments were conducted on flies with intact cuticles. Flies
680   were reared in the dark, transferred to retinal food, and tethered as described above. For optogenetic
681   experiments, a fiber-coupled LED was controlled by a T-cube LED driver (Thorlabs, LEDD1B) to deliver light
682   to the fly's head in closed-loop with its behavior. For activation of Orco+ sensory neurons, a 660 nm (red)
683   LED (Thorlabs M660FP1) was turned on (0.863 μW/mm^2) when the animal was inside the fictive odor
684   plume. For EPG inhibition experiments, a 530 nm (green) LED (Thorlabs M530F2) was turned on (0.752
685   μW/mm^2) for the duration of the entire trial.

686

687   **Closed loop parameters**: Behavioral measurements (sampled at 60 Hz) were determined by the rotation
688   of the foam ball and obtained from FicTrac (x position, y position, heading, roll, pitch and yaw). These
689   were saved alongside MFC flow values, experimental variables (odor on, LED on) and a timestamp in a
690   single .log file.

691

692   **Edge-tracking behavioral assays:** Tethered behavioral assays were conducted in a dark, climate-
693   controlled room (25-27 °C, 40-60% relative humidity). Additionally, the closed-loop olfactory system was
694   enclosed in a black tarpaulin as a further shield from other potential light sources, such as computer
695   monitors and indicator lights on system hardware. To prevent odor build-up in the enclosed space a
696   vacuum line (60 cm/s) was placed at the back of the enclosure as an exhaust. Unless otherwise stated, all
697   experiments started with a 2–5-minute baseline period in which flies walked in clean air delivered in
698   closed loop. At the end of this baseline period, flies were placed at the center of the odor plume's short
699   axis, with the exception of the 90-degree plume in which flies were placed at the center of the odor
700   plume's long axis. The geometry of the plume (0, 45-, 90-degree) was determined prior to the start of the
701   experiment. Unless otherwise stated, each plume's short axis measured 50 mm and long axis 1000 mm.
702   For EPG and FC2 imaging experiments the plume's short axis was 10 mm. For the jumping plume
703   experiments in Fig. 2h, 3e and Extended Data. Fig 5h, 6f, the edge of the plume was shifted 20 mm in the
704   direction opposite to the fly's heading as the fly exited the plume. Due to the propensity of flies to engage
705   in straighter trajectories due to the heat of the two-photon laser[39], during functional imaging of FC2
706   neurons (Fig. 6), once the fly had made 20 plume entries, the plume was jumped 3 mm on every third
707   subsequent entry. For all experiments, trials were terminated if one of three criteria were met: 1) The fly
708   traveled the length of the long axis of the plume provided (1000 mm); 2) The fly traveled over 500 mm
709   perpendicular to the plume's edge; 3) The fly traveled 100 mm downwind from its starting position on the
710   plume.

711

712   A small fraction of tethered flies (<10%) did not acclimate to walking on the ball or did not show a
713   behavioral response to ACV (by turning upwind and increasing their speed) and were excluded from the
714   study.

715

Odor concentration gradient plumes: Gradient plumes were created with the same dimensions (50 mm by 1000 mm) but featured one of three odor concentration gradients:

Vertical plume with increasing upwind odor concentration: Odor concentration increased linearly in the upwind direction, starting at 10% ACV at the plume's downwind end (0 mm) and reaching 100% ACV at the upwind end (1000 mm). **Vertical plume with decreasing upwind odor concentration:** Odor concentration decreased linearly in the upwind direction, starting at 100% ACV at the downwind end (0 mm) and diminishing to 10% ACV at the upwind end (1000 mm). **90-degree plume with crosswind odor concentration gradient:** Odor concentration varied linearly along the lateral axis, increasing from 10% to 100% ACV in one crosswind direction or decreasing from 100% to 10% ACV in the opposite direction. Flies were initially positioned at the interface between these two gradients, allowing them to track up or down the concentration gradient in the crosswind direction.

Optogenetically generated fictive odor plumes: Fictive odor plumes were the same dimensions as a vertical odor plume (50 mm by 1000 mm). Flies were positioned in the center of the plume's short axis and optogenetic stimulation was provided via a 660 nm LED whenever the fly was within the plume's boundaries.

Disappearing plumes: Flies tracked a constant concentration plume for 10 minutes. After this period, during their first trajectory outside the plume, the plume was removed, leaving the fly walking in closed-loop wind without further olfactory input.

Replay experiments in which the odor sequence was replayed back to the fly in open loop: For odor replay assays, we allowed flies to track a 90-degree plume for 10 minutes and recorded the timestamps of odor onset and offset in a separate log file. This file was used to generate the temporal sequence of odor pulses delivered during the replay epoch of the experiment which was initiated 10 sec after the edge-tracking epoch back to the same fly. The same temporal sequence of odor pulses was also presented to a naïve fly that had never edge tracked. Consequently, for every replay experiment, we collected data from one naïve fly and each naïve fly received a distinct temporal sequence of odor pulses defined by the matched replay experiment. During replay, wind was delivered in closed-loop but the animal's fictive position had no impact on the timing of odor delivery.

Operant training paradigm: The operant training paradigm consisted of three phases:

1. Initial edge-tracking phase: Flies were allowed to track a 45-degree plume. After tracking for 250 mm along the plume's edge, the plume disappeared as flies were on their next outside trajectory.
2. Operant training phase: During training, a fly's average heading and speed was continuously calculated over a 2 sec sliding window. Flies triggered the delivery of odor when their average heading was in a 45-degree range of entry angles (either -90° to -135° or 90° to 135° depending on whether training was in the same direction as the initial plume or in the opposite direction, see **Extended Data Fig. 11a**) while sustaining an average speed of > 2 mm/sec . Odor was delivered for a minimum of 2 sec and terminated when animals oriented in the 90-degree range of upwind exit angles (-45° to 45°) while sustaining an average speed of >2 mm/sec. The number of training epochs (e.g. one or five odor stimulation periods) during this training phase and whether they were in the same or opposite direction as the initial plume segment was determined prior to the start of the experiment.
3. Test edge-tracking phase: After completing the predetermined number of training epochs, flies were positioned at the center of the short axis of the test plume, oriented opposite to the

762   direction of the 45-degree plume they had tracked during the initial phase. Note that after flies
763   completed this training phase, they had to enter the test odor using the same heading as used for
764   the training phase and so effectively had an additional epoch of reinforcement. In the test phase,
765   the plume extended 20 mm below the fly's starting position to increase the chances that they
766   successfully entered the test plume.

767

768 **Analyses of edge tracking behavior**
769 **Trajectory averages (Fig. 1e, 2e-h, Extended Data Fig. 5d, 6a):** To construct average trajectories, x and y
770 coordinates for each outside or inside bout were upsampled to contain 10,000 points through linear
771 interpolation between data points using the pandas library in Python. This allowed us to average x and y
772 coordinates regardless of the length of the inside or outside bout. Upsampled x and upsampled y
773 coordinates were averaged to produce one set of (x,y) coordinates for each animal. To construct an
774 average across animals, the averages generated from individual animals were averaged together.

775

776 **Entry and exit angles:** Entry and exit angles were determined by calculating the mean traveling direction
777 in the 0.5 sec prior to and 0.5 after crossing the plume's boundary.

778

779 **Analysis of inbound and outbound segments (Fig. 1f, Extended Data Fig. 5d):** The outside trajectories of
780 flies tracking a vertical plume were simplified into straight line segments using the Ramer-Douglas-
781 Peucker (RDP) algorithm,[75] which simplifies a set of x, y coordinates by iteratively reducing the number of
782 points in the trace. The parameter ε determines the maximum allowed distance between the simplified
783 and original trajectories and was 1 mm. These trajectories were then averaged using the linear
784 interpolation method described above providing a single average trajectory for each animal. From this
785 average trajectory, "outbound" (away from the edge) and "inbound" (back towards the edge) path lengths
786 were calculated as follows: (1) outbound pathlength was calculated as the pathlength from the point of
787 exiting the plume to the farthest point orthogonal to the plume's edge and (2) inbound pathlength was
788 calculated as the pathlength from the farthest point orthogonal to plume's edge back to the plume's
789 boundary. These three points – plume exit point, farthest point and plume entry point – define a triangle,
790 the interior angles of which define inbound and outbound angles as indicated in Fig. 1f. For analyses of
791 simulated inbound and outbound trajectories in a random search model (Extended Data Fig. 5d), we took
792 the total number of outside bouts for each fly and then randomly selected the same number of outside
793 simulated outside trajectories. From this collection of random trajectories, we used the method above to
794 generate an average trajectory and then calculated outbound/inbound lengths.

795

796 **Anemotaxis definition (Fig. 6e):** Trajectories of animals prior to ACV exposure (pre-air period) were
797 divided into anemotaxis bouts, defined in a similar manner to menotaxis bouts in (Mussels-Pires et al
798 2024). Animals' trajectories were simplified into straight line segments using the Ramer-Douglas-Peucker
799 algorithm (epsilon = 10 mm). Segments of length greater than 50 mm were assigned as anemotaxis bouts.

800

801 **Random-walk model (Fig. 1g, Extended Data Fig. 5):** We simplified the outside trajectories of 40 flies
802 tracking a vertical plume using the Ramer-Douglas-Peucker algorithm (epsilon=1 mm) and extracted the
803 straight-line distances (run lengths) that flies traveled between successive turns and the angles between
804 consecutive straight-line vectors (turn angles) to capture the changes in heading direction at each turn
805 and stored each in a separate library.

806 We simulated random-walk trajectories by randomly sampling from the two empirical distributions of run
807 lengths and turn angles. Simulated flies started at the plume's edge and the initial run length was assigned

808 a heading that was randomly drawn from the initial segment heading directions from the plume (**Extended**
809 **Data Fig. 5b**). At each step:

810   1. A run length was randomly sampled from the empirical distribution of run lengths.
811   2. A turn angle was randomly sampled from the empirical distribution of turn angles.
812   3. The simulated fly moved forward by the run length and then adjusted its heading by the turn
813   angle.

814 The simulation continued until the simulated fly either re-encountered the plume edge or exceeded a
815 maximum distance traveled 500 mm in the direction perpendicular to the plume's edge which is the same
816 maximum distance flies were allowed to travel in experiments before a trial was terminated.

817 To reflect the natural tendency of flies to walk upwind even in the absence of odor cues[16], we modified
818 the random-walk model to include an upwind bias. We adjusted the turn direction based on a sinusoidal
819 probability function whose magnitude scaled between 0 and 1 [value a]. When a=0, the probability of
820 turning left or right is the same for all heading directions. As the values of a increase from a=0 to a=1, the
821 fly becomes progressively more biased to turn left when it is facing right, and to turn right when facing
822 left. The value of a was selected to match that of real flies (**Extended Data Fig. 5c**) mirroring the upwind
823 bias observed in actual flies outside the odor plume.

824 Given that random exploration outside the plume should not depend on the geometry of the plume
825 tracked, the same model was used to simulate outside trajectories for flies tracking the 45-degree and 90-
826 degree plume, drawing from same empirically-derived libraries of run lengths and turn angles (**Extended**
827 **Data Fig. 5**). The only difference between the models was the initial heading which was sampled from
828 the initial segment heading directions for the 45- and 90-degree trajectories.

829 **Functional imaging:** All functional imaging experiments were performed on either an Ultima or
830 Investigator two-photon laser scanning microscope (Bruker) equipped with galvanometers driving a
831 Chameleon Ultra II Ti:Sapphire laser. Emitted fluorescence was detected with GaAsP photodiode
832 (Hamamatsu) detectors. Images were acquired with an Olympus 40X, 0.8 NA or 20X, 1.0 NA objective at
833 512 pixels × 512 pixels resolution. The laser was tuned to 920 nm for all experiments. The out-of-objective
834 power for all experiments was ~15mW and never exceeded 25 mW. For volumetric imaging, 3-5 slices
835 were recorded using a piezoelectric Z-focus (Bruker) at a rate of 3-10 Hz.
836

837 **Data alignment:** To align the imaging and behavioral data, we used a 3.3V digital pulse from a RaspberryPi
838 to initiate recording of an imaging stack through the PrairieView (Bruker) I/O interface. The RaspberryPi
839 continued to send 3.3V pulses every 10s which were recorded with PrairieView for confirmatory alignment
840 of the imaging and behavioral data. Behavioral variables were captured at 60–61 frames per second,
841 whereas neural activity (fluorescence) was captured at 3-10 frames per second. To align these two distinct
842 time series, a standardized and regular time series was generated for each trace containing 100-ms time
843 bins (0, 100, 200, 300, etc.). Behavioral data was binned at the center of each time point and averaged.
844 Imaging data was upsampled using linear interpolation at the same 100 ms time bins. Custom Python
845 scripts were used to synchronize and log incoming FicTrac variables and outgoing MFC and motor
846 commands, allowing us to align the wind direction, odor concentration, behavioral data and imaging
847 frames.
848

849 **Image registration and ROIs:** All images were stored as individual .tiff files which were registered using
850 the StackReg function of the pystackreg library. ROIs were drawn using custom Python scripts, Fij, or a

851   custom MatLab GUI. To quantify EPG neuron activity recorded from the protocerebral bridge, we followed
852   the methods described in (Lyu et al., 2022)[46] and manually defined each of the 16 glomeruli from the
853   registered stacks corresponding to each imaging plane.

855   FC2 neuron activity during edge tracking was recorded in the fan-shaped body. EPG neuron activity in the
856   ellipsoid body was recorded synchronously to allow for direct comparison of their phase relationships
857   during an experiment. To quantify FC2 neuron activity, we manually defined the lateral borders of the
858   fan-shaped body, extended these lines down to a point and divided the arc defined by these intersecting
859   lines into 16 wedges. Pixels were assigned to each wedge if they resided within the wedge and within the
860   footprint of the FC2 neurons, defined by masks that were manually drawn in each imaging layer based on
861   their arborization pattern. To quantify EPG neuron activity recorded in the ellipsoid body, we radially
862   divided the ellipsoid body into 16 sub wedges from a manually defined center. Pixels were assigned to
863   each wedge if they resided within the wedge and within the footprint of the EPG neurons, defined by
864   masks that were manually drawn in each imaging layer based on their arborization pattern.

866    $\Delta F/F_0$ values were determined by the formula $(F-F_0)/F_0$, where F is the mean pixel value within a
867   wedge/glomerulus and F_0 is the mean of the lowest 5% of F values.

869   **Neuronal phase analysis:** Phase was determined by two methods. For recordings of EPG neurons in the
870   protocerebral bridge, phase was calculated as in Green et al. 2017[44]. For each timepoint the Fourier
871   transform was taken on the $\Delta F/F_0$ activity vector of the 16 glomeruli. Phase was determined as the phase
872   of the Fourier spectrum at a period of 8, the peak periodicity of the power spectrum[44]. For recordings of
873   EPG neurons in the ellipsoid body and FC2 neurons in the fan-shaped body, phase was defined as the
874   population vector average of wedge signals as per Seelig and Jayaraman 2015; Lyu et al. 2022[37,46]. In
875   summary, the 16 wedges of the ellipsoid body and fan-shaped body were assigned angles from -180° to
876   180°, equally dividing 360° of azimuthal space. Angles were assigned so that ellipsoid body and fan-shaped
877   body wedges were in correspondence as per the connectome[49]. In the ellipsoid body, wedges were
878   counted counterclockwise starting from the most ventral wedge to the right of the midline. In the fan-
879   shaped body, wedges were counted from right to left. For each timepoint, each wedge was assigned a
880   vector with length equal to the $\Delta F/F_0$ value and direction given by its assigned angle. Phase was the angle
881   of the population vector average of these vectors at each timepoint.

883   **Phase nulling:** Phase nulled EPG signals recorded in the protocerebral bridge were calculated as
884   previously described[44,46]. At each frame, we rotated the signal by the estimated phase of the activity bump
885   in that frame, such that all bumps were aligned. To compare bumps in and out of odor, we separated
886   frames corresponding to when the fly was in or out of the odor and averaged 122 together with the signal
887   from all these frames to get the average bump amplitude.

889   **Phase calibration to allocentric coordinates:** The anatomical location of activity bumps in the central
890   complex correspond to azimuthal orientations in allocentric space. However, the mapping from
891   anatomical to external coordinates varies between animals and can remap during an experiment[37]. To
892   produce EPG and FC2 signals aligned to external coordinates, we rotated phase and wedges by an offset
893   at each timepoint such that phase angle 0° was aligned upwind and the central two wedges corresponded
894   to 22.5° to the left and right of the upwind direction (**Fig. 6c**). The offset was the rolling mean (over 2 s)
895   of the difference between the EPG phase and the animal's heading, since the EPG signal provided a faithful
896   neural correlate of heading relative to the wind (**Fig. 3b**). To rotate wedges, this offset was converted to
897   an integer value varying between -8 and 8 by rounding to the nearest 22.5°. The same offset was applied
898   to EPG and FC2 signals.

899

900 **Model**

901 **Time Discretization:** We bin the data into time intervals of 0.2 s and run the behavioral model in discrete
902 times steps with this same interval. Because we are modeling the motion of the fly, we excluded data
903 points when the fly's speed is less than 1 mm/s.

904

905 **Edge Crossing Events for Memory Update:** To avoid spurious events and to account for the finite width
906 of the odor boundary, we define an edge crossing when a fly is on one side of the odor boundary for three
907 consecutive times points and then on the other side for three consecutive time points. We define the fly's
908 velocity unit vector at the time of the crossing, $\hat{\boldsymbol{v}}$, as its velocity averaged over this five-time-step interval,
909 normalized to unit length.

910

911 **State:** The model has two states: returning and leaving. When the fly leaves the odor plume in the leaving
912 state, a time interval is drawn from a negative binomial distribution $NB(r_{\text{leave}}, 1-p_{\text{leave}})$ and, after that
913 number of time steps, the state switches to the returning state if the fly is still out of the plume. When
914 the fly enters the odor plume in the returning state, a time interval is drawn from a negative binomial
915 distribution $NB(r_{\text{return}}, 1-p_{\text{return}})$ and, after that number of time steps, the state switches to the leaving state
916 if the fly is still in the plume. Otherwise, no transitions occur. The parameters r_{leave}, p_{leave}, r_{return} and p_{return}
917 are determined by fitting to data by the procedure describe below.

918

919 **Memory:** The model stores 2-d vector memories of plume exit and entry directions. The entry memory
920 vector $\boldsymbol{m}_{\text{entry}}$ is updated at the time of each entry by

921 $$\boldsymbol{m}_{\text{entry}} \leftarrow a_{\text{entry}}\boldsymbol{m}_{\text{entry}} + b_{\text{entry}}\hat{\boldsymbol{v}} + \boldsymbol{\epsilon}_{\text{entry}}$$

922 where $\hat{\boldsymbol{v}}$ is the entry velocity unit vector defined above, and the two components of $\boldsymbol{\epsilon}_{\text{entry}}$ are random
923 variables drawn from a normal distribution with zero mean and variance σ^2_{entry}. The exit memory vector
924 $\boldsymbol{m}_{\text{exit}}$ is updated at the time of each exit by

925 $$\boldsymbol{m}_{\text{exit}} \leftarrow a_{\text{exit}}\boldsymbol{m}_{\text{exit}} + b_{\text{exit}}\hat{\boldsymbol{v}} + \boldsymbol{\epsilon}_{\text{exit}}$$

926 with $\hat{\boldsymbol{v}}$ the exit velocity unit vector and $\boldsymbol{\epsilon}_{\text{exit}}$ drawn from a normal distribution with zero mean and
927 variance σ^2_{exit}. In simulations, we ignore updates for which the exit $\hat{\boldsymbol{v}}$ is more than $60°$ away from the
928 upwind direction. This follows the intuition that flies have an innate tendency to exit upwind. Other than
929 during these plume boundary crossings, $\boldsymbol{m}_{\text{entry}}$ and $\boldsymbol{m}_{\text{exit}}$ remain unchanged. The values of the memory
930 vectors at the beginning of a trajectory depend on unknown previous history. We model $\boldsymbol{m}_{\text{entry}}(0)$ as the
931 null vector and $\boldsymbol{m}_{\text{exit}}(0)$ with a trajectory-specific Gaussian prior $N(\boldsymbol{\mu}_0, \sigma^2_0 I)$ during fitting.

932

933 The parameters a_{entry}, b_{entry}, σ^2_{entry}, a_{exit}, b_{exit}, σ^2_{exit}, $\boldsymbol{\mu}_0$ and σ^2_0 are determined by the fitting procedure
934 described below. During fitting, nonzero values of σ^2_0, σ^2_{entry} and σ^2_{exit} allow unexplained variation of
935 latent memories. However, during simulation, we set $\sigma^2_0 = \sigma^2_{\text{entry}} = \sigma^2_{\text{exit}} = 0$ to test the effectiveness
936 of our hypotheses without introducing extra noise into the memories. When simulating from models fitted
937 to a single trajectory, as in Extended Data Fig. 6d, we set the initial exit memory to $\boldsymbol{\mu}_0$. When simulating
938 from the average fly model (parameters computed from multiple trajectories; **Fig. 5b**), we set the upwind
939 component of the initial exit memory to a fixed value $w_{\parallel}$ equal to the median of the upwind components
940 of $\boldsymbol{\mu}_0$ from all training trajectories, and we sample the crosswind component from a uniform distribution
941 over the range from $-2w_{\perp}$ to $+2w_{\perp}$, where $w_{\perp}$ is the median of the absolute value of the crosswind
942 components of $\boldsymbol{\mu}_0$ from all training trajectories.

943

944 **Velocity update:** In the leaving state, velocity is updated at every time step with a decay term, a bias
945 towards the current exit memory, and a noise term,

22

946 $$v(t) = c_{\text{leave}} v(t-1) + (1 - c_{\text{leave}}) m_{\text{exit}} + \xi_{\text{leave}}(t)$$

947 with $\xi_{\text{leave}}(t)$ drawn from a Gaussian distribution with zero mean and variance σ^2_{leave}. Similarly, in the
948 returning state, the velocity update is

949 $$v(t) = c_{\text{return}} v(t-1) + (1 - c_{\text{return}}) m_{\text{entry}} + \xi_{\text{return}}(t)$$

950 with $\xi_{\text{leave}}(t)$ drawn from a Gaussian distribution with zero mean and variance σ^2_{return}.

951

952 **Variational Inference and Parameter Learning:** For each trajectory, we compute the variational
953 distributions of latent variables and trajectory-specific parameters using coordinate ascent of the
954 evidence lower bound[51,52,76]. For r>1, state transitions can be implemented in a Markov chain with an
955 expanded state space, where each original state is augmented with $r - 1$ additional super states. The
956 parameters r and p, for both the leaving and returning states, can then be updated by fitting a negative
957 binomial distribution to samples from the variational distribution of states[76]. For simplicity, we set $r = 1$
958 during all but the final iteration of the fitting algorithm.

959

960 For the average fly model, we fit a single set of optimal parameters (except for μ_0 and σ^2_0, which are still
961 trajectory specific) to latent variable distributions calculated using the above procedure from the 28
962 trajectories with no less than 30 returns (**Extended Data Fig. 7c,h**). We chose a relatively large threshold
963 on the number of returns to provide a high number of data points for determining the memory update
964 parameters.

965

966 For the average fly model, $w_\parallel$ = 6.299 mm/s, and $w_\perp$ = 1.695 mm/s, and, as shown in **Extended Data Figure**
967 **7c**:

968

	entry memory	exit memory
a	0.727	0.956
b	0.437mm/s	0.482mm/s
	return after entry	leave after exit
r	2	1
p	0.505	0.81
	returning state	leaving state
c	0.733	0.6
σ	3.23 mm/s	3.255 mm/s

969

970 **Comparison with data:** We remove odor changes lasting only 1 or 2 time steps for simulated trajectories
971 before comparing to fly data, which matches the data preprocessed to remove odor changes lasting less
972 than 0.5s.

973

974

975 **References:**

976 1. Baker, K. L. *et al.* Algorithms for Olfactory Search across Species. *Journal of Neuroscience* **38**, 9383–9389
977   (2018).
978 2. Reddy, G., Murthy, V. N. & Vergassola, M. Olfactory Sensing and Navigation in Turbulent Environments.
979   *Annu Rev Condens Matter Phys* **13**, 191–213 (2022).
980 3. Webb, B. & Wystrach, A. Neural mechanisms of insect navigation. *Curr Opin Insect Sci* **15**, 27–39 (2016).
981 4. Heinze, S. Unraveling the neural basis of insect navigation. *Curr Opin Insect Sci* **24**, 58–67 (2017).

982   5.   Wehner, R. *Desert Navigator*. (Harvard University Press, 2020).

983   6.   Emonet, T. & Vergassola, M. Olfactory cues and memories in animal navigation. *Nature Reviews Physics* **6**,
984   215–216 (2024).

985   7.   Murthy, V. N. Olfactory navigation in fluctuating environments. *Curr Biol* **34**, R1013–R1018 (2024).

986   8.   Murlis, J., Elkinton, J. S. & Carde, R. T. Odor plumes and how insects use them. *Annu Rev Entomol* **37**, 505–
987   532 (1992).

988   9.   Álvarez-Salvado, E. *et al.* Elementary sensory-motor transformations underlying olfactory navigation in
989   walking fruit-flies. *Elife* **7**, (2018).

990   10.   Kennedy, J. S. & Marsh, D. Pheromone-regulated anemotaxis in flying moths. *Science* **184**, 999–1001
991   (1974).

992   11.   van Breugel, F. & Dickinson, M. H. Plume-Tracking Behavior of Flying Drosophila Emerges from a Set of
993   Distinct Sensory-Motor Reflexes. *Current Biology* **24**, 274–286 (2014).

994   12.   Connor, E. G., McHugh, M. K. & Crimaldi, J. P. Quantification of airborne odor plumes using planar laser-
995   induced fluorescence. *Exp Fluids* **59**, 137 (2018).

996   13.   Wehner, R. The architecture of the desert ant's navigational toolkit. *Myrmecol News* **12**, 85–96 (2009).

997   14.   Crimaldi, J. P. & Koseff, J. R. High-resolution measurements of the spatial and temporal scalar structure of a
998   turbulent plume. *Exp Fluids* **31**, 90–102 (2001).

999   15.   Handler, A. *et al.* Distinct Dopamine Receptor Pathways Underlie the Temporal Sensitivity of Associative
1000   Learning. *Cell* **178**, (2019).

1001   16.   Zolin, A. *et al.* Context-dependent representations of movement in *Drosophila* dopaminergic reinforcement
1002   pathways. *Nat Neurosci* **24**, pages 1555–1566 (2021).

1003   17.   Cardé, R. T. & Willis, M. A. Navigational strategies used by insects to find distant, wind-borne sources of
1004   odor. *J Chem Ecol* **34**, 854–866 (2008).

1005   18.   Mafra-neto, A. & Carde, R. T. Orientation of Flying Moths. **369**, 142–144 (1994).

1006   19.   Murlis, J., Willis, M. A. & Cardé, R. T. Spatial and temporal structures of pheromone plumes in fields and
1007   forests. *Physiol Entomol* **25**, 211–222 (2000).

1008   20.   Webster, D. R. & Weissburg, M. J. Chemosensory guidance cues in a turbulent chemical odor plume. *Limnol
1009   Oceanogr* **46**, 1034–1047 (2001).

1010   21.   Borst, A. & Heisenberg, M. Osmotropotaxis in *Drosophila melanogaster*. *J Comp Physiol* **147**, 479–484
1011   (1982).

1012   22.   Kadakia, N. *et al.* Odour motion sensing enhances navigation of complex plumes. *Nature* **611**, 754–761
1013   (2022).

1014   23.   Louis, M., Huber, T., Benton, R., Sakmar, T. P. & Vosshall, L. B. Bilateral olfactory sensory input enhances
1015   chemotaxis behavior. *Nat Neurosci* **11**, 187–199 (2008).

1016   24.   Riman, N., Victor, J. D., Boie, S. D. & Ermentrout, B. The Dynamics of Bilateral Olfactory Search and
1017   Navigation. *SIAM Review* **63**, 100–120 (2021).

1018   25.   Tobin, T. R. & Bell, W. J. Chemo-orientation of male Trogoderma variabile (Coleoptera, Dermestidae) in a
1019   simulated corridor of female sex pheromone. *Journal of Comparative Physiology A* **158**, 729–739 (1986).

1020   26.   Willis, M. A. & Avondet, J. L. Odor-modulated orientation in walking male cockroaches Periplaneta
1021   americana, and the effects of odor plumes of different structure. *Journal of Experimental Biology* **208**, 721–
1022   735 (2005).

1023   27.   Zimmer-Faust, R. K., Finelli, C. M., Pentcheff, N. D. & Wethey, D. S. Odor plumes and animal navigation in
1024   turbulent water flow: A field study. *Biological Bulletin* **188**, 111–116 (1995).

1025   28.   Bell, J. S. & Wilson, R. I. Behavior Reveals Selective Summation and Max Pooling among Olfactory
1026   Processing Channels. *Neuron* **91**, 425–438 (2016).

1027   29.   Tao, L., Ozarkar, S. & Bhandawat, V. Mechanisms underlying attraction to odors in walking *Drosophila*. *PLoS
1028   Comput Biol* **16**, e1007718 (2020).

1029   30.   Kennedy, J. S. Zigzagging and casting as a programmed response to wind-borne odour: a review. *Physiol
1030   Entomol* **8**, 109–120 (1983).

1031   31.   Kalmus, H. Anemotaxis in *Drosophila*. *Nature* **150**, 405 (1942).

1032   32.   Mussells Pires, P., Zhang, L., Parache, V., Abbott, L. F. & Maimon, G. Converting an Allocentric Goal into an
1033   Egocentric Steering Signal. *Nature* **626,** 808-818 (2024).

33. Dethier, V. G. The Hungry Fly: A Physiological Study of the Behavior Associated with Feeding. Harvard University Press (1976).

34. Kim, I. S. & Dickinson, M. H. Idiothetic Path Integration in the Fruit Fly *Drosophila melanogaster*. *Current Biology* **27**, 2227-2238.e3 (2017).

35. Wittlinger, M., Wehner, R. & Wolf, H. The ant odometer: Stepping on stilts and stumps. *Neuroforum* **12**, 240–241 (2006).

36. Singh, S. H., van Breugel, F., Rao, R. P. N. & Brunton, B. W. Emergent behaviour and neural dynamics in artificial agents tracking odour plumes. *Nat Mach Intell* **5**, 58–70 (2023).

37. Seelig, J. D. & Jayaraman, V. Neural dynamics for landmark orientation and angular path integration. *Nature* **521**, 186–191 (2015).

38. Fisher, Y. E., Lu, J., Alessandro, I. D. & Wilson, R. I. Sensorimotor experience remaps visual input to a heading-direction network. (2019) *Nature* **576**, 121–125 (2019).

39. Green, J., Vijayan, V., Mussells Pires, P., Adachi, A. & Maimon, G. A neural heading estimate is compared with an internal goal to guide oriented navigation. *Nat Neurosci* **22**, 1460–1468 (2019).

40. Kim, S. S., Hermundstad, A. M., Romani, S., Abbott, L. F. & Jayaraman, V. Generation of stable heading representations in diverse visual scenes. *Nature* **576**, 126–131 (2019).

41. Okubo, T. S., Patella, P., D'Alessandro, I. & Wilson, R. I. A Neural Network for Wind-Guided Compass Navigation. *Neuron* **107**, 924-940.e18 (2020).

42. Giraldo, Y. M. *et al.* Sun Navigation Requires Compass Neurons in *Drosophila*. *Current Biology* **28**, 2845-2852.e4 (2018).

43. Westeinde, E. A. *et al.* Transforming a head direction signal into a goal-oriented steering command. *Nature* **626**, 819–826 (2024).

44. Green, J. *et al.* A neural circuit architecture for angular integration in *Drosophila*. *Nature* **546**, 101–106 (2017).

45. Turner-Evans, D. *et al.* Angular velocity integration in a fly heading circuit. *Elife* **6**, e23496 (2017).

46. Lyu, C., Abbott, L. F. & Maimon, G. Building an allocentric travelling direction signal via vector computation. *Nature* **601**, 92-97 (2022)

47. Lu, J. *et al.* Transforming representations of movement from body- to world-centric space. *Nature* **601**, 98-104 (2022)

48. Stone, T. *et al.* An Anatomically Constrained Model for Path Integration in the Bee Brain. *Current Biology* **27**, 3069-3085.e11 (2017).

49. Hulse, B. K. *et al.* A connectome of the Drosophila central complex reveals network motifs suitable for flexible navigation and context-dependent action selection. *Elife* **10**, (2021).

50. Dan, C., Hulse, B. K., Kappagantula, R., Jayaraman, V. & Hermundstad, A. M. A neural circuit architecture for rapid learning in goal-directed navigation. *Neuron* **112**, 2581-2599.e23 (2024).

51. Ghahramani, Z. & Hinton, G. E. Variational Learning for Switching State-Space Models. *Neural Comput.* **12**, 831–864 (2000).

52. Zoltowski, D., Pillow, J. & Linderman, S. A general recurrent state space framework for modeling neural dynamics during decision-making. PMLR **119**:11680-11691 (2020).

53. Currier, T., Matheson, A. & Nagel, K. A population of central complex neurons promoting airflow-guided orientation in *Drosophila*. *Elife* **9**, 6510 (2020).

54. Kathman, N. D., Lanz, A. J., Freed, J. D. & Nagel, K. I. Neural dynamics for working memory and evidence integration during olfactory navigation in *Drosophila*. bioRxiv (2024). 10.1101/2024.10.05.616803

55. Matheson, A. M. M. *et al.* A neural circuit for wind-guided olfactory navigation. *Nat Commun* **13**, 4613 (2022).

56. Aso, Y. *et al.* Neural Circuit Mechanisms for Transforming Learned Olfactory Valences into Wind-Oriented Movement. *Elife* **12** 85756 (2023).

57. Jacobs, L. F. From chemotaxis to the cognitive map: The function of olfaction. *Proc Natl Acad Sci U S A* **109**, 10693–10700 (2012).

58. McKissick, O., Klimpert, N., Ritt, J. T. & Fleischmann, A. Odors in space. *Front Neural Circuits* **18**, (2024).

59. Zeppilli, S. *et al.* Mammalian olfactory cortex neurons retain molecular signatures of ancestral cell types. *bioRxiv* (2023) doi:10.1101/2023.08.13.553130.

1086   60.   Poo, C., Agarwal, G., Bonacchi, N. & Mainen, Z. F. Spatial maps in piriform cortex during olfactory
1087   navigation. *Nature* **601**, 595–599 (2022).
1088   61.   Fischler-Ruiz, W. *et al.* Olfactory landmarks and path integration converge to form a cognitive spatial map.
1089   *Neuron* **109**, 4036-4049.e5 (2021).
1090   62.   Collett, M. & Collett, T. S. How does the insect central complex use mushroom body output for steering?
1091   *Current Biology* **28**, R733–R734 (2018).
1092   63.   Collett, M., Collett, T. S., Bisch, S. & Wehner, R. Local and global vectors in desert ant navigation. *Nature*
1093   **394**, 269–272 (1998).
1094   64.   Kadakia, N., Anderson, H. D., Clark, D. A. & Emonet, T. Walking *Drosophila* navigate complex plumes using
1095   stochastic decisions biased by the timing of odor encounters. *Elife* **9**, 1–31 (2020).
1096   65.   Nagel, K. I. & Wilson, R. I. Biophysical mechanisms underlying olfactory receptor neuron dynamics. *Nat
1097   Neurosci* **14**, 208–216 (2011).
1098   66.   Cafaro, J. Multiple sites of adaptation lead to contrast encoding in the *Drosophila* olfactory system. *Physiol
1099   Rep* **4**, 1–14 (2016).
1100   67.   Gorur-Shandilya, S., Demir, M., Long, J., Clark, D. A. & Emonet, T. Olfactory receptor neurons use gain
1101   control and complementary kinetics to encode intermittent odorant stimuli. *Elife* **6**, e27670 (2017).
1102   68.   Vergassola, M., Villermaux, E. & Shraiman, B. I. 'Infotaxis' as a strategy for searching without gradients.
1103   *Nature* **445**, 406–409 (2007).
1104   69.   Singh, S. H., van Breugel, F., Rao, R. P. N. & Brunton, B. W. Emergent behaviour and neural dynamics in
1105   artificial agents tracking odour plumes. *Nat Mach Intell* **5**, 58–70 (2023).
1106   70.   Baier, H. & Bonhoeffer, F. Axon guidance by gradients of a target-derived component. *Science* **255**, 472–
1107   475 (1992).
1108   71.   Geva-Sagiv, M., Las, L., Yovel, Y. & Ulanovsky, N. Spatial cognition in bats and rats: from sensory acquisition
1109   to multiscale maps and navigation. *Nat Rev Neurosci* **16**, 94–108 (2015).
1110   72.   Honkanen, A., Adden, A., Da Silva Freitas, J. & Heinze, S. The insect central complex and the neural basis of
1111   navigational strategies. *Journal of Experimental Biology* **222**, (2019).
1112   73.   Maimon, G., Straw, A. D. & Dickinson, M. H. Active flight increases the gain of visual motion processing in
1113   Drosophila. *Nat Neurosci* **13**, 393–399 (2010).
1114   74.   Moore, R. J. D. *et al.* FicTrac: A visual method for tracking spherical motion and generating fictive animal
1115   paths. *J Neurosci Methods* **225**, 106–119 (2014).
1116   75.   Douglas, David. H. & Peucker, T. K. Algorithms for the reduction of the number of points required to
1117   represent a digitized line or its caricature. *Cartographica* **10**, 112–122 (1973).
1118   76.   Linderman, S., Antin, B., Zoltowski, D., & Glaser, J. SSM: Bayesian learning and inference for state space
1119   models. *github* (2020).
1120

Acknowledgements:

1132
1133
1134

Author contributions:

A.S. and C.M. designed and performed all behavioral experiments with odor plumes. N.E. performed behavioral experiments using optogenetic activation of sensory neurons. A.S. performed functional recordings of EPG neurons. C.D. performed functional recordings of FC2 neurons. S.M. and L.F.A developed, implemented, and analyzed the model. A.S., S.M., C.D., N.E., J.R. L.F.A and V.R contributed to analyzing and interpreting the data. V.R. wrote the manuscript with input from all the authors.

Correspondence:

Correspondence to Vanessa Ruta (ruta@rockefeller.edu).

Competing Interests:

The authors declare no competing interests.

Supplementary Information:

Supplementary Video 1: Representative video of a fly navigating within the closed loop olfactory paradigm. The fly walks on an air-supported ball with a tube carrying clean air/odor yoked to its angular heading.

Supplementary Video 2: Video of a representative fly tracking the edge of a vertical plume. Right: view from the back of the fly walking on an air-supported ball with the air/odor tube in front. Middle: Expanded view of fly trajectory as it crosses the border of the fictive odor plume. Right: Trajectory of fly mapped onto 1 meter plume.

Supplementary Video 3: Video of a representative fly tracking a jumping plume. Boundaries of plume shown in white lines, which jump 20 mm in the opposite direction of the fly's heading each time the fly exits. Fly trajectory shown in magenta.
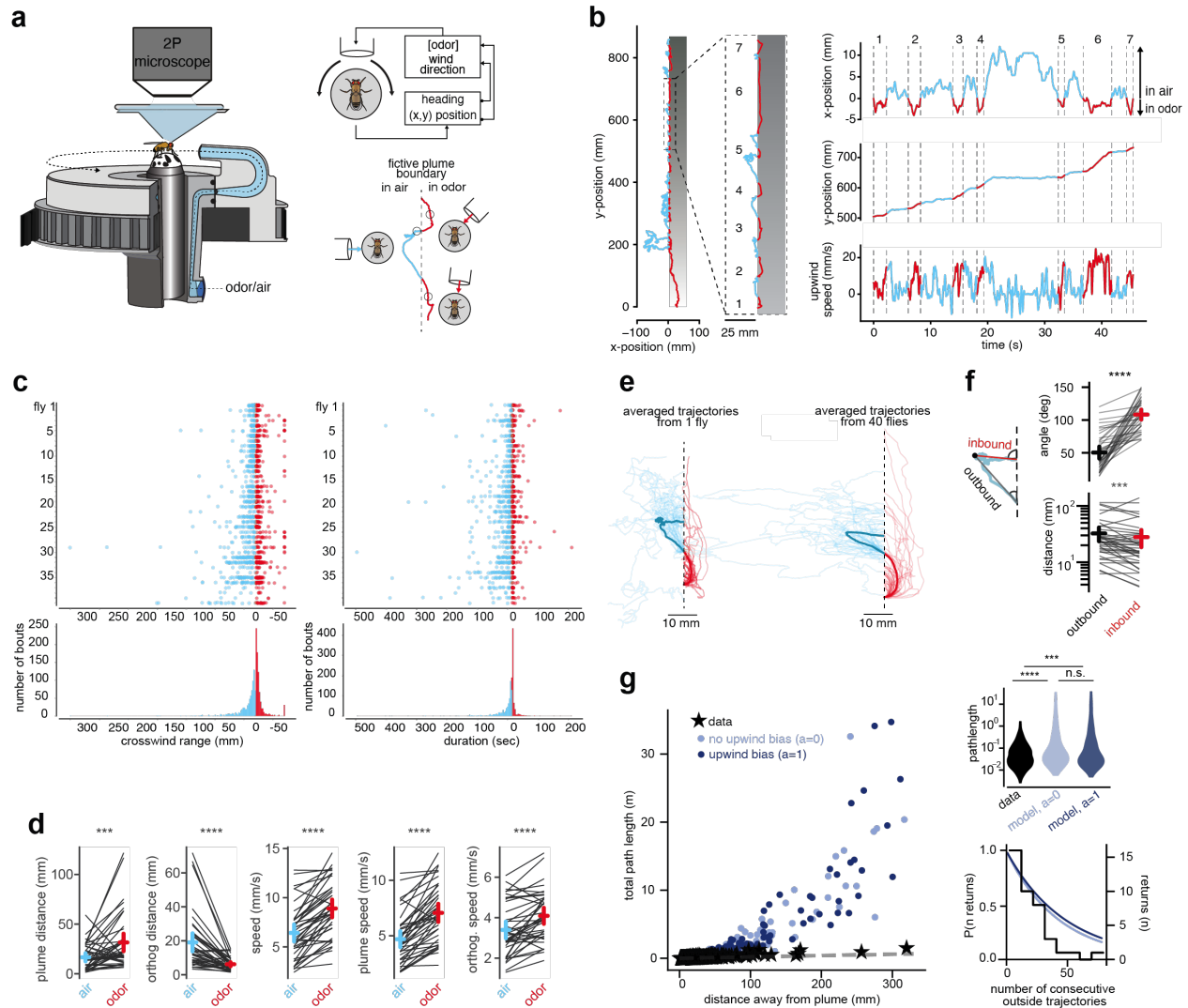
Figure 1: A virtual reality system for olfactory navigation (a) Left: Schematic of the closed loop virtual reality system for plume navigation in which a tethered, walking fly's heading on an air-supported ball is used to control the angular position of a nozzle delivering a constant airstream, with or without odor. Right, above: The fly's fictive position is used to control the odor concentration delivered through the airstream. Right, below: Schematic depicting how the position of the airstream and odor concentration change as a head-fixed fly navigates across the fictive plume boundary (dashed line). Trajectory is red when the fly is in the odor and blue outside the odor corridor. **(b)** Left: an example trajectory of a fly tracking a 50 mm wide odor corridor with an ascending gradient (10-100% apple cider vinegar over 1 m). Trajectory is red when the fly is in the odor and blue outside the odor corridor, with enlarged view of the highlighted segment delineated by dashed box. Right: x-position (crosswind axis), y-position (upwind axis), and upwind speed for the inside/outside bouts shown in the highlighted segment. **(c)** Distribution of crosswind distances (left) and durations (right) for the inside and outside bouts of 40 flies. Each dot represents a single bout inside the odor corridor (red) or outside the odor in clean air (blue). **(d)** Comparison of average behavioral metrics for all bouts inside the odor (red) or outside the odor in clean air (blue). Plume distance refers to distance traveled along the longitudinal plume axis while orthogonal distance refers to distance traveled orthogonal to the plume. Each line represents the average for all inside or outside bouts for an individual fly, with the average across flies ±S.E.M. shown in red or blue. n=40 flies. **(e)** Aligned trajectories inside (red) and outside (blue) the plume. Left: all trajectories (thin lines) for the fly shown in (b) and the scaled average for that individual (thick line). Right: Aligned scaled average trajectories for 40 flies (thin lines) and average across all animals (thick line). **(f)** Comparison of the inbound and outbound segments of outside trajectories, defined as leading away from (outbound, black) or returning to (inbound, red) the point farthest from the plume in the crosswind direction (see Methods). Top right: Angles between outbound and inbound segments and plume as depicted in schematic at left. Bottom: Pathlength of outbound and inbound segments, plotted on logarithmic scale. Each thin line represents the average for all trajectories of an individual fly, with the inter-individual average ±S.E.M. shown. n=40 flies. **(g)** The total pathlength

of an outside bout as a function of crosswind distance away from the plume for fly data (black stars) or a random-walk model (see Methods and Extended Data Fig. 5) with (dark blue) and without an upwind bias (light blue). Dashed line represents maximal possible efficiency (e.g. when the pathlength is twice the crosswind distance indicating a straight path away from the plume and back through the shortest pathlength). Right top: the distribution of path lengths from real flies (black) and random models, without an upwind bias (dark blue) and with upwind bias (light blue). Right bottom: the probability of returning for n consecutive returns with data from real flies (black) and random models, without an upwind bias (dark blue) and with upwind bias (light blue). n=755 outside trajectories from 40 flies and 755 simulated trajectories. n.s. not significant; ***p < 0.001; ****p < 0.0001. Details of statistical analyses and sample sizes are given in Table S1.
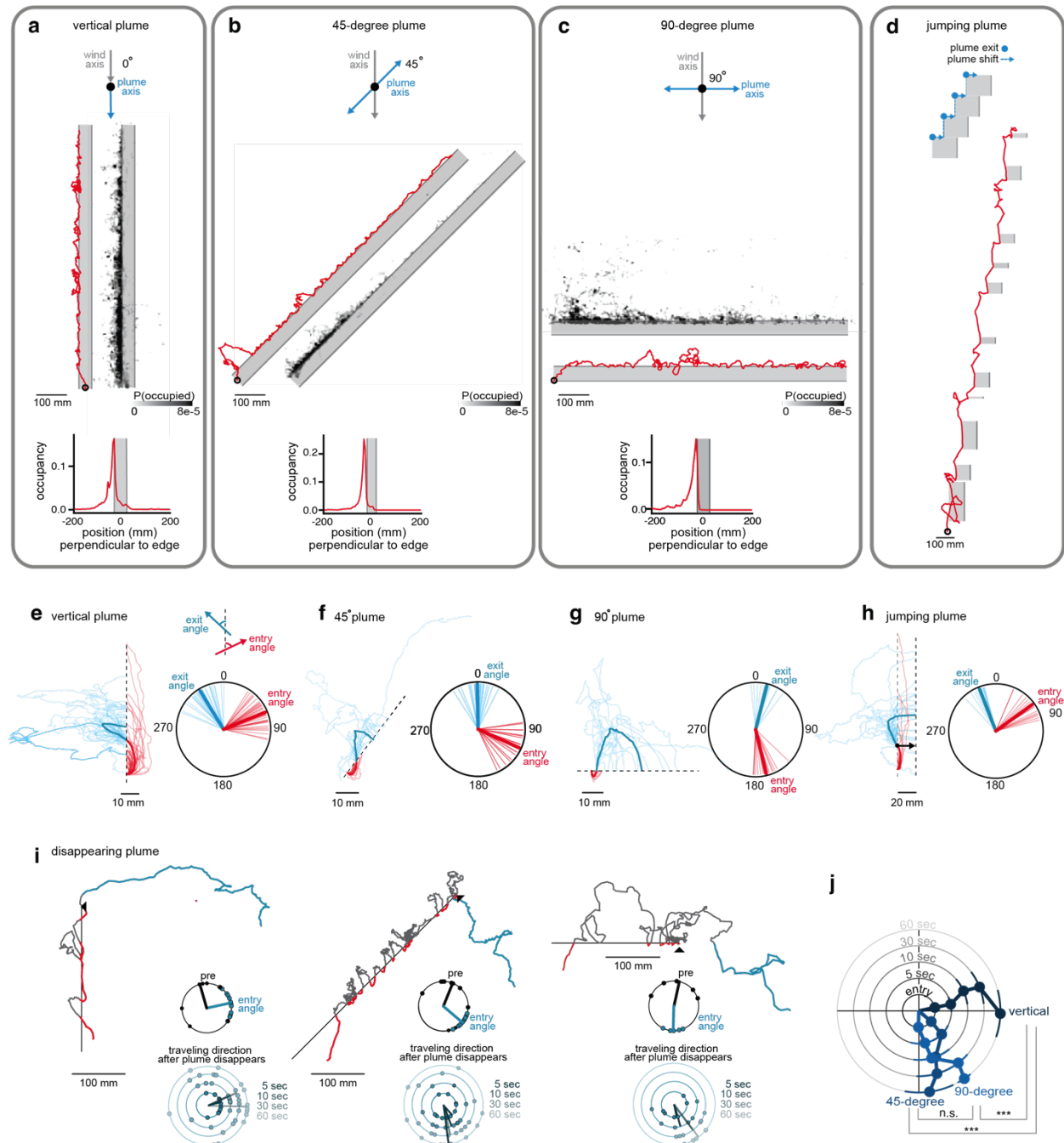
Figure 2: Flies track plumes that are not aligned with the wind. (a-c) Flies track plumes with different orientations relative to the wind. For each plume type, we show a single representative trajectory (red, with starting position denoted by black circle); heatmap in greyscale depicting occupancy, and occupancy as a function of distance perpendicular to the plume. **(a)** n=40 flies; **(b)** n=21 flies; **(c)** n=20 flies. **(d)** Representative trajectory of a fly navigating a 'jumping' plume where the plume shifts 20 mm to the right, each time the fly exits the plume. Trajectory is shown in red with starting position denoted by black circle. **(e)-(h)** Left: aligned and averaged inside and outside trajectories for each plume orientation. Each thin line represents the scaled average for a single individual and the thick line represents the average across all individuals. Right: distribution of entry and exit angles for each plume type. Each thin line represents the average for all exits and entries from a single fly and the thick line represents average across all individuals. **(e)** n=40 flies; **(f)** n=21 flies; **(g)** n=20 flies; **(h)** n=24 flies. Entry and exit angles were determined by calculating the mean heading in the 0.5 sec prior to and 0.5 sec after crossing the plume's boundary as shown in (e). **(i)** Trajectories of flies after the plume vanishes while the fly is on outside bout the plume for 0-degree (vertical), 45-degree and 90-degree plume. For each plume orientation, a representative example is shown

with the plume's boundary indicated by black line, and inside bouts shown in red and outside bouts in grey. The point at which the plume disappears is indicated by the black arrowhead, with the fly's trajectory over the next two minutes shown in blue. For each, top polar plot shows the distributions of average heading direction while animals walked in closed loop wind in the absence of odor during the two minutes prior to plume tracking (pre, black) and average entry angle during plume tracking (blue). Bottom polar plot shows the average heading direction at indicated times after the plume's disappearance. Each dot represents an individual fly with vertical n=12 flies; 45-degree n=11 flies; 90-degree n=6 flies. **(j)** Comparison of the average entry angle during plume tracking (innermost circle) and traveling direction for the indicated times after the plume's disappearance for all flies in (i). Each circle reflects the indicated time bin, with mean and SEM shown. Details of statistical analyses and sample sizes are given in Table S1. n.s., not significant, ***p < 0.001. Details of statistical analyses and sample sizes are given in Table S1.
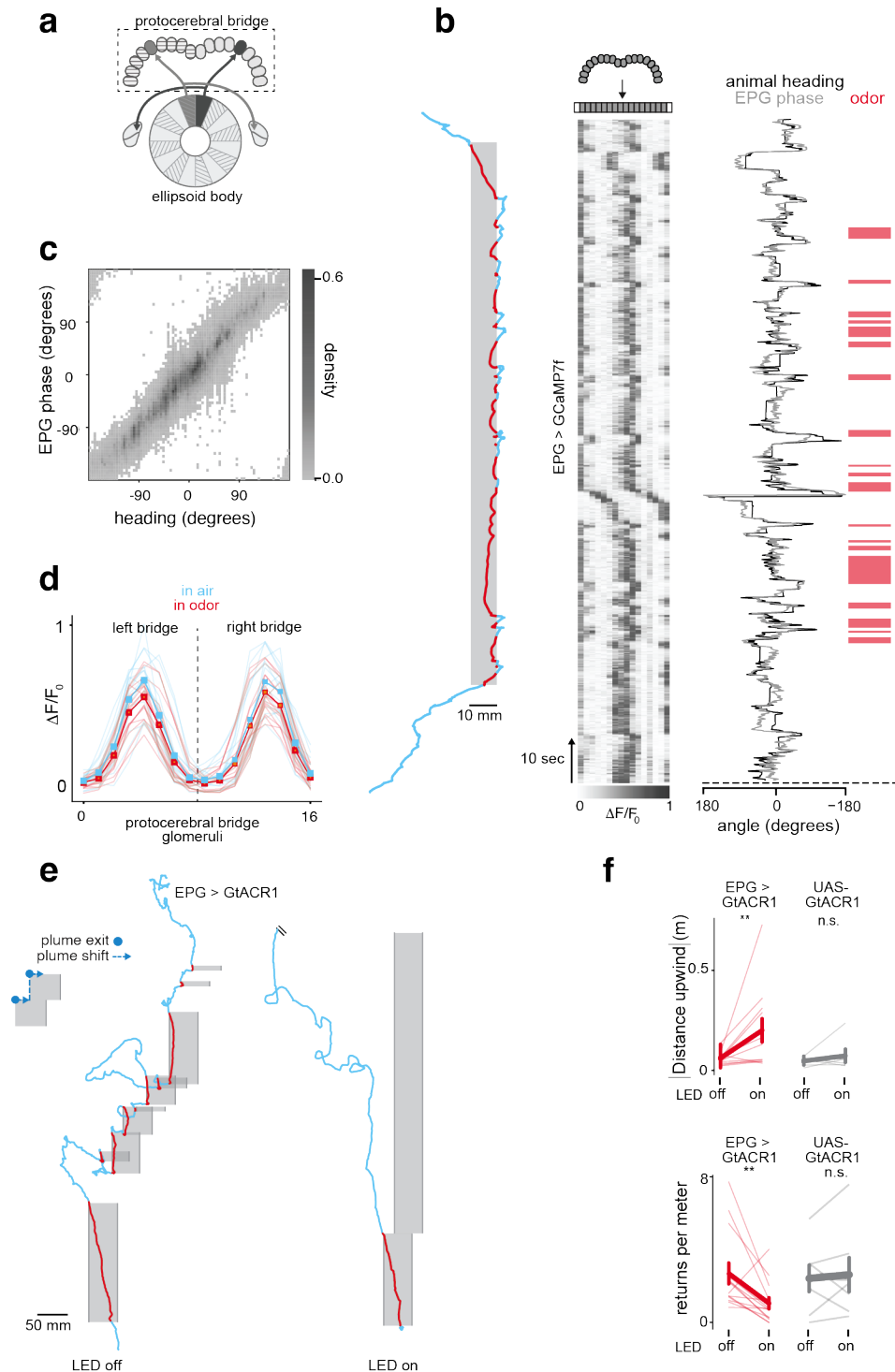
Figure 3: EPG neurons represent a fly's heading and are required for edge tracking. (a) Schematic of the central complex neuropils innervated by EPG neurons. Adjacent EPG neurons in the ellipsoid body project to glomeruli in the left and right protocerebral bridge. **(b)** Representative recording of EPG activity as a fly edge tracks a 10 mm wide vertical plume. Left: trajectory of an individual fly, with inside bouts shown in red and outside bouts in blue. Middle: Heatmap of EPG activity ($\Delta F/F_0$) during edge tracking. Each column in the heatmap represents EPG activity in 16 glomeruli in the protocerebral bridge as indicated at top. Right: alignment of the EPG phase estimate (grey) with the animal's heading (black) during this same edge-tracking trial. Timing of in odor bouts are depicted in red at

far right. **(c)** Heat-map representing the correspondence between an animal's heading and the estimated phase of the EPG bump during edge tracking. N=16 trials from 9 animals. **(d)** The amplitude of phase-offset activity bumps in the left and right protocerebral bridge during edge tracking when the animal is walking in the odor (red) or in air (blue). N=16 trials from 9 animals. **(e)** Representative experiment showing the trajectory of an EPG>GtACR fly navigating a jumping plume in the absence (left) and presence (right) of optogenetic inhibition via LED illumination throughout the edge-tracking trial. **(f)** Comparison of distance traveled upwind upon re-encountering the plume (top) and number of successful return trajectories (bottom) for EPG>GtACR and UAS-GtACR control flies in the absence and presence of optogenetic inhibition. Each thin line represents an individual fly, with thick line showing mean across flies and SEM. n.s., not significant, **p < 0.01. Details of statistical analyses and sample sizes are given in Table S1.
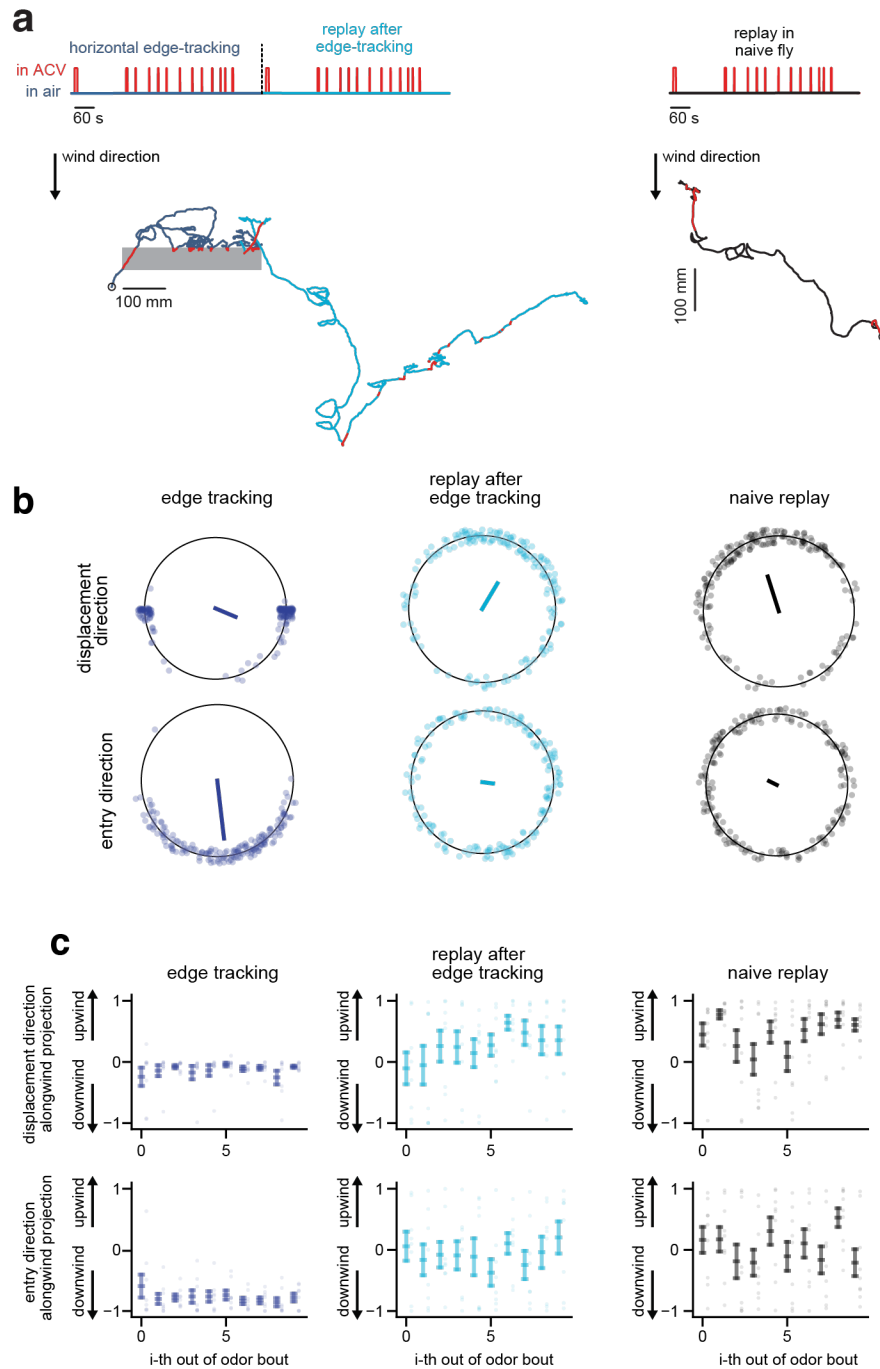
Figure 4: Fly trajectories depend on the spatial structure of their olfactory experience. (a) Left: Representative 'replay' experiment in which a fly was allowed to edge track along a 90° plume for 10 minutes, after which the same temporal sequence of odors was presented back to the same fly. Schematic on top depicts the sequence of odor encounters during edge tracking that was replayed to the fly during the replay epoch. Representative trajectory during edge tracking shown as red in odor and dark blue when outside the odor, while trajectory during replay epoch is red inside the odor and cyan when outside the odor. Right: Trajectory of a naïve animal when presented with the same odor sequence. **(b)** Polar plots showing the net displacement direction when flies are outside the odor (top,) and entry direction when they encounter the odor (bottom) during edge tracking (left, dark blue), replay to the same fly (middle, cyan), or replay in naïve animals (right, black). Each point represents a single bout for an individual fly, with average vector for all flies shown as a line. n=8 flies. **(c)** The displacement direction and entry direction of flies over sequential outside bouts of edge tracking trials (left, dark blue), replay of the odor sequence to the same flies

34

(middle, cyan), and replay of the odor sequence to a naïve flies (right, black). n=8 flies. The alongwind projection is shown, with 1 denoting straight upwind and -1 denoting straight downwind, to emphasize the change in the direction of outside bouts depending on the conditions in which the fly encounters the odor.
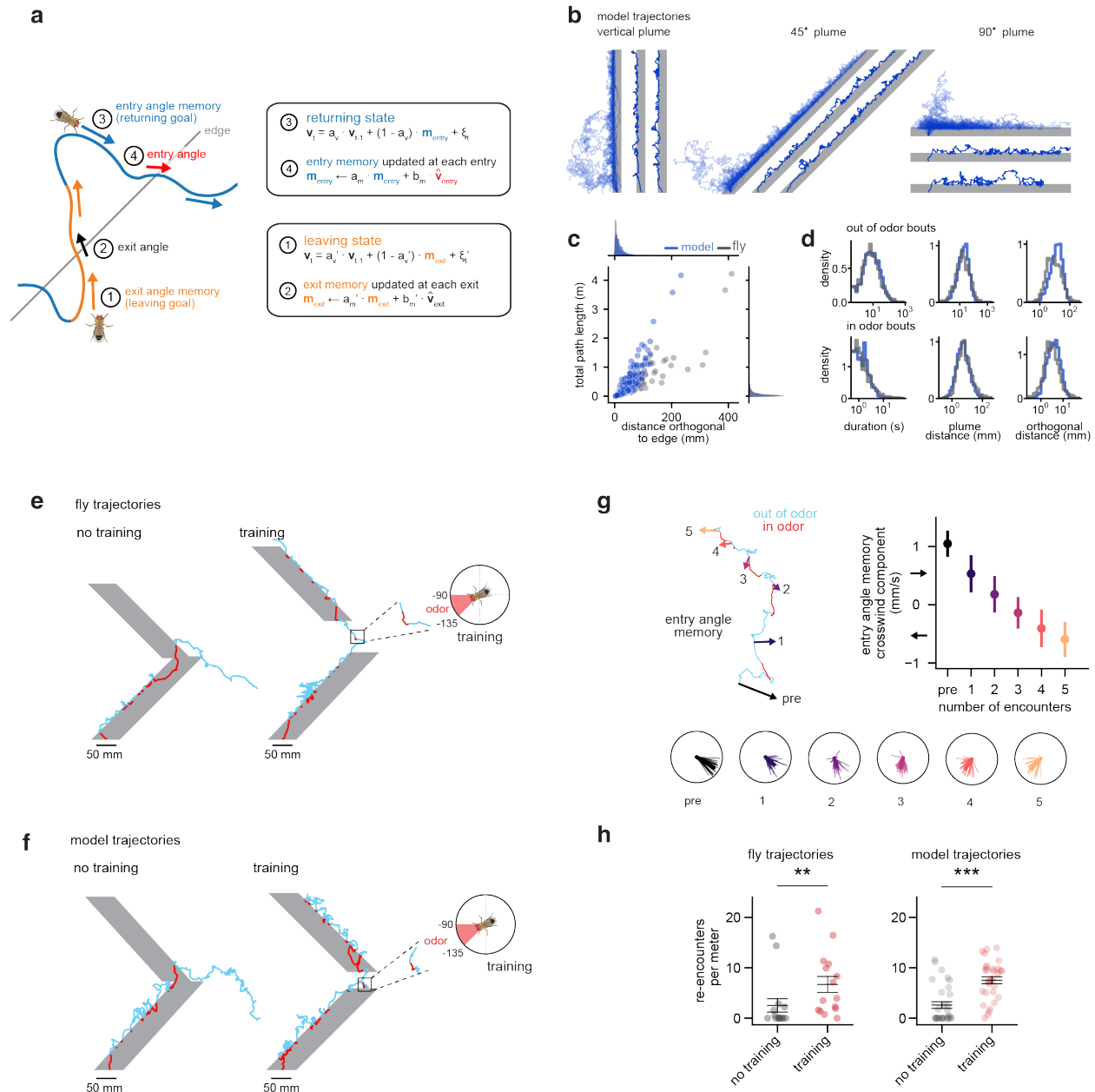
Figure 5: A behavioral model of edge tracking suggests flies rapidly update their entry angle memories with experience. (a) Components of the switching space model mapped onto a schematized trajectory of a fly tracking the edge (gray) of a 45-degree plume. When the fly is in the leaving state (orange), it relies on its exit angle memory (m_{exit}) which it updates each time it exits the plume (black arrow). When the fly is in the returning state (blue), it relies on its entry angle memory (m_{entry}) which it updates each time it enters the plume (red arrow). **(b)** Representative individual trajectories simulated from the model shown for plumes with different geometries relative to the wind. For each plume, two trajectories are shown individually (dark lines) or an overlay of 25 trajectories (semi-transparent lines). **(c)** Comparable efficiency of simulated and real fly trajectories revealed by plotting total path length versus total distance in the direction perpendicular to the plume's boundary for 72 animals and 75 simulations tracking 0-,45-, and 90-degree plumes. Each dot represents a single outside bout. **(d)** Histograms comparing metrics across population of 72 flies tracking 0-,45-, and 90-degree plumes (gray) or across 75 simulated trajectories (blue). **(e)** Left: Representative trajectory of a naïve fly provided with two 45-degree plume segments demonstrating that in the absence of training (left), flies continue to progress in the direction required to re-enter the first plume segment. Right: A single operant training session (see Methods), in which a fly was exposed to odor when it spontaneously walked in the direction required to enter the second plume segment (-90° to -135°), was sufficient to enable the fly to subsequently track a 45-degree plume segment oriented in the opposite direction.

Note that to enter the second plume segment flies must travel in the same direction as used for operant conditioning (-90° to -135°) and so effectively have a second operant training epoch. **(f)** Model simulations of the same experiment shown in (e). **(g)** Top left: Simulation showing how the entry angle memory gradually shifts over multiple odor encounters during operant training paradigm shown in (e), transitioning from pointing to the lower right after tracking the first 45-degree segment to pointing to the lower left. Top right: a plot of the crosswind component of entry angle memory as a function of number of odor encounters during operant training, n=29 simulations, mean +/- std deviation. Bottom: entry angle memory vectors as a function of odor encounters during operant training for same 29 simulations, with individual simulations (thin lines) and average vector (thick line). **(h)** A single operant training trial enhances the ability to track a 45-degree plume segment oriented in the other direction. Shown is the number of plume re-encounters on the second segment 45-degree plume of both real (left) and model (right) flies. **p < 0.01, ***p < 0.001. Details of statistical analyses and sample sizes are given in Table S1.
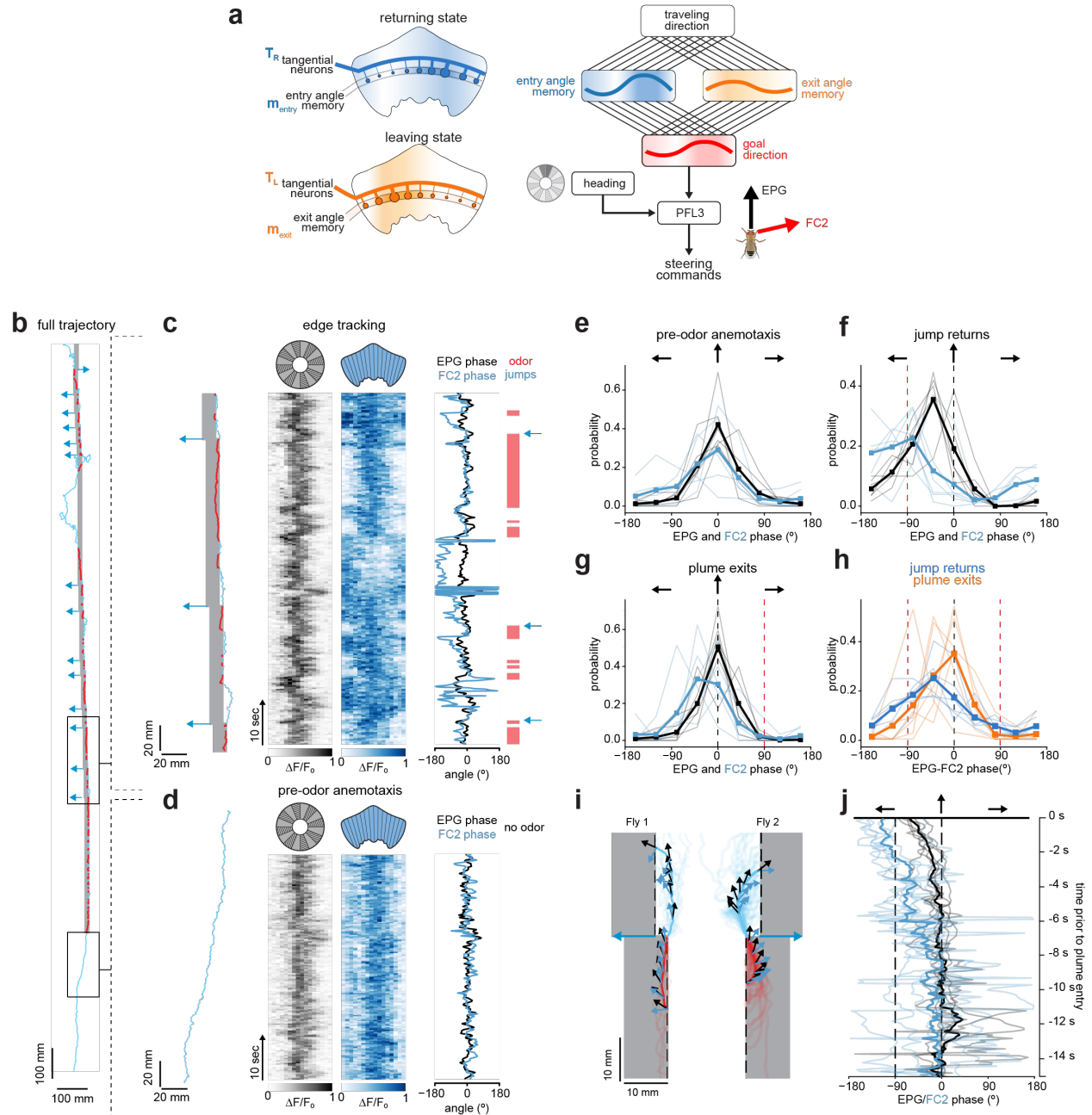
Figure 6: FC2 neurons signal the direction of the plume's boundary prior to returns. (a) Left: Schematic of circuitry in the fan-shaped body hypothesized to store entry and exit angle memories. Memories are stored in synapses between state-activated tangential neurons and columnar neurons encoding traveling direction. Right: Schematic of the full model. Crossing the plume's boundary drives the storage of an entry or exit angle memory that is alternately read out in the returning or leaving states. Memory is conveyed to FC2 neurons representing the fly's goal direction, and this direction is compared to the fly's current heading by the PFL neurons that drive corrective steering to align the fly's current heading with its goal. **(b)** Representative experiment in which the activity of FC2 neurons in the fans-shaped body and EPG neurons in the ellipsoid body are synchronously recorded as a fly walks in clean air and then tracks the edge of a 10 mm wide jumping plume. After the first 20 entries to the plume, the plume is periodically jumped 3 mm away from the fly during returns (as indicated by blue arrows) to minimize the chance of incidental returns back to the plume's boundary. **(c)** Epoch of edge tracking corresponding to the highlighted region in (b). Left: Trajectory of the fly as it exits and re-enters the plume. Middle: EPG and FC2 activity ($\Delta F/F_0$) for that edge-tracking epoch plotted by wedge in the ellipsoid body for EPG neurons (greyscale) and by column in the fan-shaped body for FC2 neurons (bluescale). Right: Estimated EPG (black) and FC2 (blue) phases for that epoch with an indication of when the fly is in the odor (red) and when the plume is jumped (blue arrows). **(d)** Same as for (c) but for the epoch

when the same fly was walking upwind prior to encountering the odor plume corresponding to the lower boxed region in (b). **(e)** Distributions of EPG phases (black) and FC2 phases (blue) during upwind walking (anemotaxis). Thin lines represent individual flies and thick lines represent mean across flies. n=6 flies. Distributions are centered around the upwind direction. **(f)** Distributions of EPG and FC2 phases in the 1 sec prior to returns to the jumped plume. Distributions are skewed toward the plume boundary (crosswind direction to the boundary indicated by vertical dashed line). **(g)** Distributions of EPG and FC2 phases in the 0.5 sec prior to exiting of the plume, corresponding to the epochs immediately prior to the returns shown in (f). Direction to the boundary indicated by vertical dashed line. **(h)** Distribution of the difference between EPG and FC2 phases during jumped returns (as in panel (f), orange) and exits (as in panel (g, blue). Crosswind direction towards the plume boundary indicated by the left dashed line and crosswind direction away from plume indicated by right dashed line. Note FC2 phase leads EPG phase in the direction of the odor boundary during returns. n =6 flies. **(i)** Representative mean EPG phase (black arrows) and FC2 phase (blue arrows) plotted as direction vectors onto the averaged exit and return trajectories for two flies that were tracking different sides of the plume. Transparent lines correspond to individual trajectories. Phase is plotted at 12 evenly spaced points on an interpolated time base (6 points inside the plume, 6 points outside the plume). **(j)** Mean progression of EPG phases (black) and FC2 phases (blue) in the 15 sec prior to when flies returned to the plume after a jump. Thin lines represent individual flies, n=6 flies. Bold lines represent mean across flies. n=6 flies. Crosswind direction towards plume boundary indicated by dashed line.
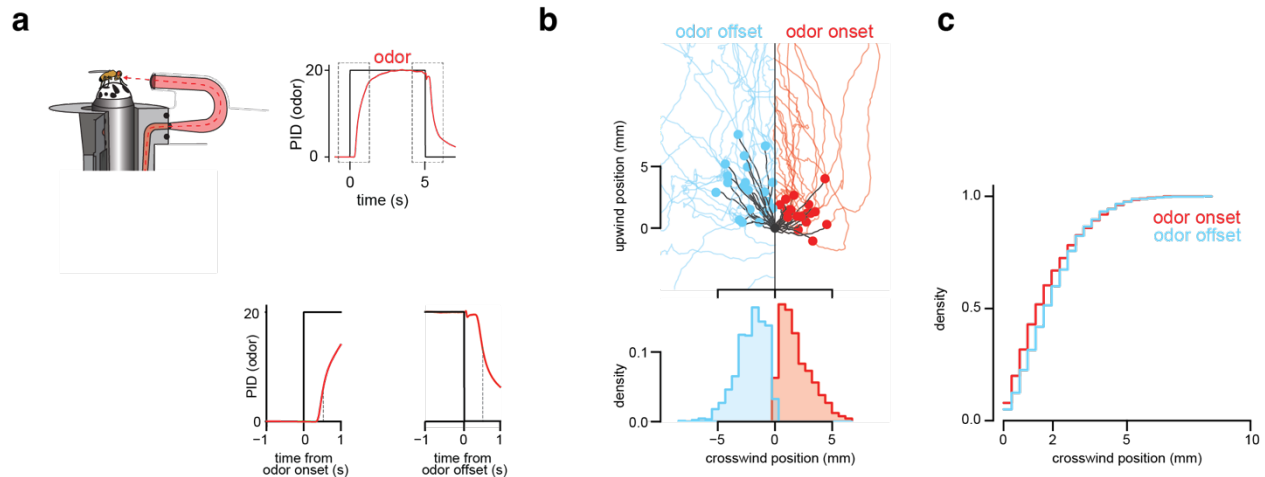
Extended Data Figure 1: Characteristics of odor stimulation at the plume's boundary (a) Left: Schematic of closed-loop olfactory system highlighting nozzle yoked to the fly's heading that provides a continuous stream of clean air, infused with odor (apple cider vinegar) when fly is inside the boundary of the fictive plume. Right: odor concentration profiles measured by PID (photoionization detector) over time at the position of the fly. Top panel shows the full duration of an odor pulse with an onset and decay of approximately 500 msec. Bottom panels show zoomed-in views of the PID trace over the first second from odor pulse onset (left) and offset (right). **(b)** Positional data of a representative fly upon odor onset and offset. Top: the position of the fly for all entries into the plume (red) and exits from the plume (blue). The solid points represent the animal's position 500 msec after odor onset and offset. Bottom: histogram shows the distribution of crosswind positions of the fly upon exiting the plume (blue) and upon entering the plume (red). Due to the finite time required for the odor to reach the fly as it walks in virtual space shown in (a), the plume's edge is not perfectly sharp, with a spatial gradient that depends on how fast the fly is walking. **(c)** Cumulative density functions (CDFs) of crosswind positions for flies in response to plume entry (red) and exit (blue). n=40 flies, 731 inside trajectories and 796 outside trajectories.
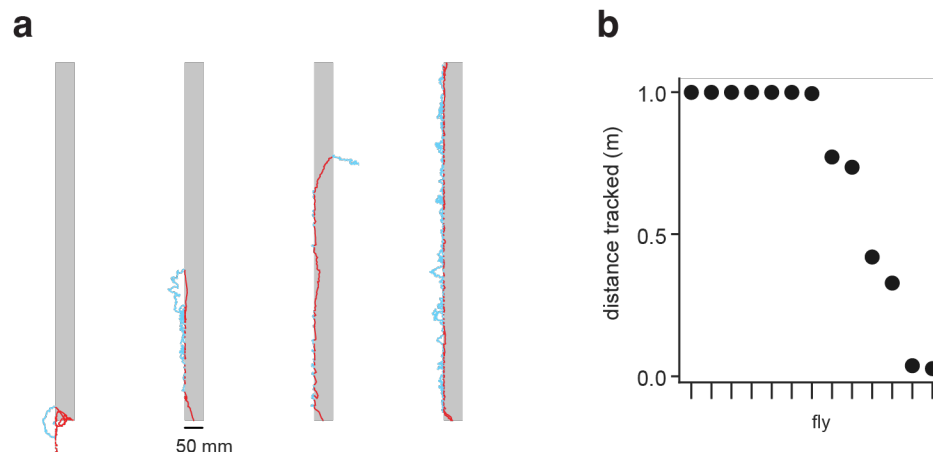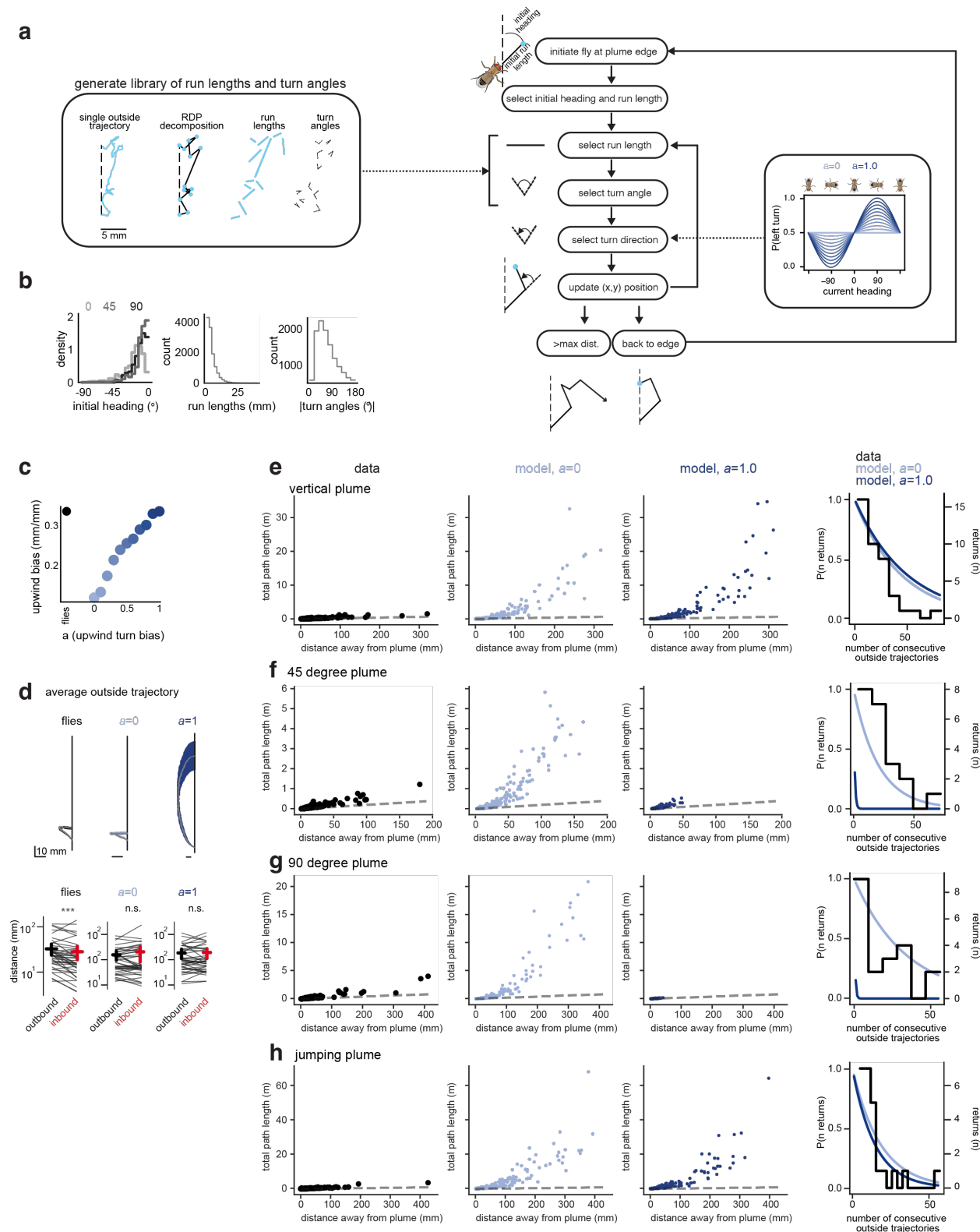

Extended Data Figure 2: Flies readily edge track along the edge of a vertical plume. (a) Representative trajectories of four naïve flies that had never previously encountered an odor corridor tracking a 1-meter vertical plume. Epochs outside the plume are depicted in blue and epochs inside the plume are depicted in red. **(b)** Plume distance tracked by 13 naïve flies. Note that for these experiments, the trial was terminated once a fly tracked more than 1 meter upwind, more than 500 mm in the crosswind direction or more than 100 mm downwind after encountering the plume.

40
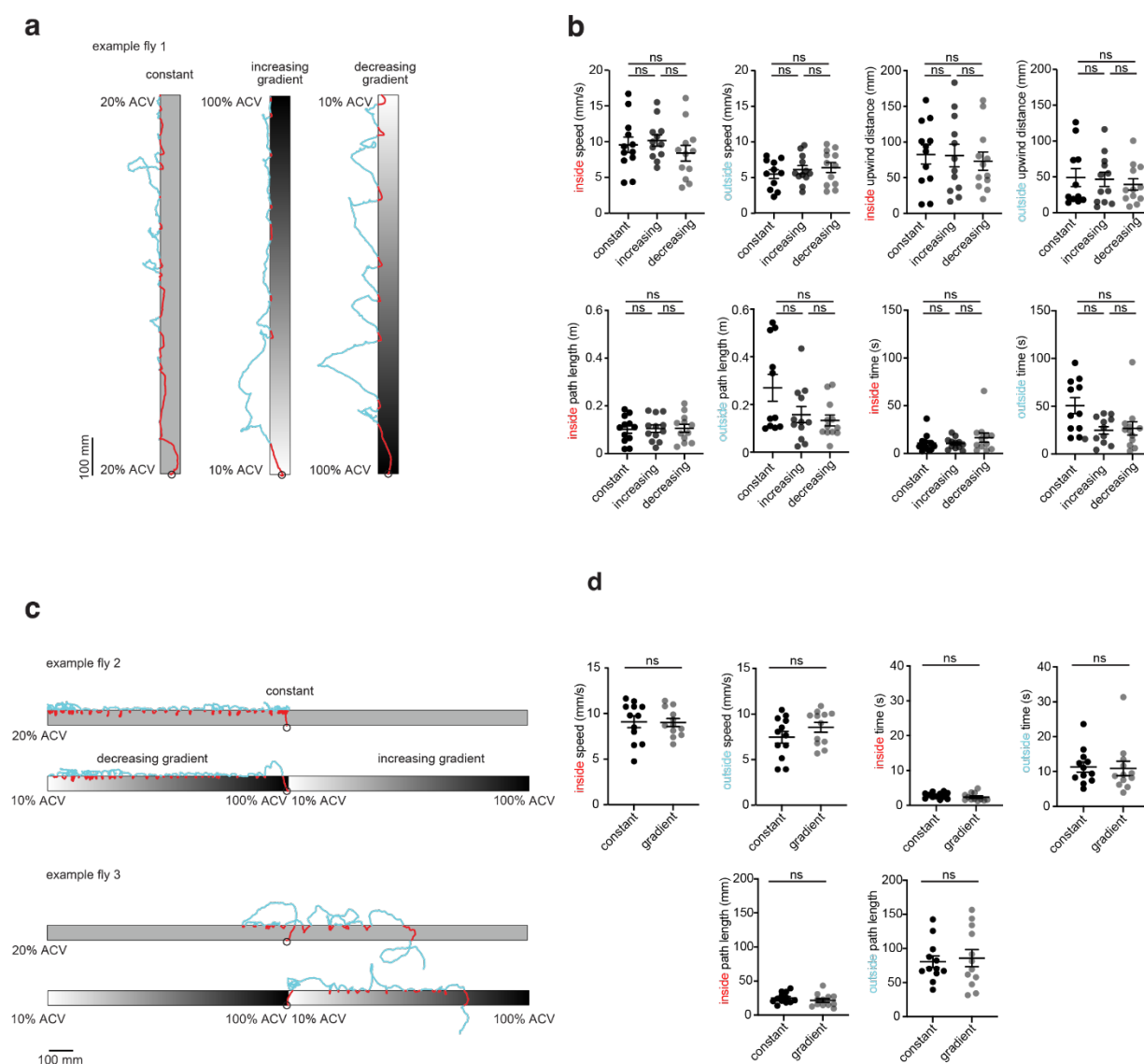
Extended Data Figure 3: Edge tracking does not depend on the concentration gradient along the longitudinal axis of the plume. (a) Representative trajectories of an individual fly tracking an odor corridor of a constant concentration of 20% apple cider vinegar (ACV) (left), a plume with an increasing ACV concentration gradient in the upwind direction (10-100% ACV over 1-meter, middle) and a plume with a decreasing ACV concentration gradient in the upwind direction (100-10% ACV over 1-meter, right). Start of each trajectory is marked with a circle. **(b)** Comparison of average behavioral metrics for the three plumes shown in (a). Each fly navigated a constant concentration, increasing gradient and decreasing gradient plume in a randomized order across flies. Each point represents the average metrics for a single fly, with interindividual average and SEM shown (n = 12 flies). Wilcoxon signed rank test. **(c)** Representative trajectories for two flies that sequentially navigated a constant concentration 90-degree plume (top) and 90-degree plume, in which the fly was positioned at the center and could select to walk up an increasing (10-100% ACV over 1-meter) or decreasing gradient (100-10% ACV over 1-meter, bottom). **(d)** Comparison of average behavioral metrics for the constant or gradient plumes shown in (c). Each point represents the average metrics for a single fly, with interindividual average and SEM shown (n = 12 flies). n.s. not significant, p > 0.05. Details of statistical analyses and sample sizes are given in Table S1.

41
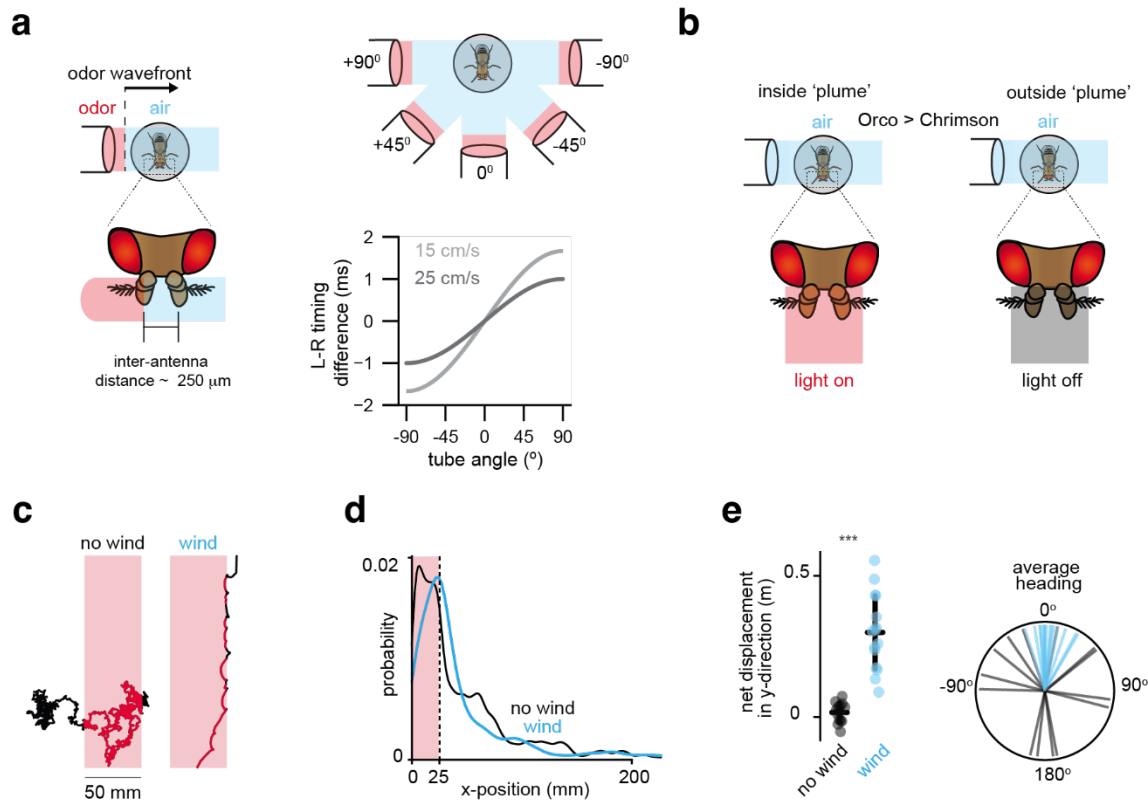
Extended Data Figure 4: Flies do not appear to require bilateral signals to localize the plume's edge or track along its boundary. (a) Schematic of the experimental setup in closed-loop olfactory stimulation paradigm illustrating the contact timing of an odor wavefront arriving from different angles (+90°, +45°, 0°, -45°, -90°) to each antenna. Given the small spatial distance between the two antennae and the speed of the air flow, the difference in the timing of odor arrival is < 1 ms even when animals are walking in the crosswind direction. **(b)** Schematic of experimental setup for flies navigating a fictive odor plume generated by optogenetic activation of Orco+ sensory neurons expressing CsChrimson. When a fly is inside the boundaries of the fictive odor plume (left), both antennae are simultaneously stimulated using 660 nm light. Outside the fictive plume (right), the light is off (grey) and there is no stimulation. Wind is maintained in closed loop throughout. **(c)** Representative trajectories of a fly presented with a 660 nm light corridor in the absence (left) or presence (right) of wind. Paths inside the corridor are shown in red while paths outside the corridor are shown in black. **(d)** Probability distributions of the absolute value of flies' x-positions inside a light corridor (depicted in red) in the presence (blue) or absence of wind (black). n=14 flies (no wind), 15 flies (wind). **(e)** Left: Average displacement in the y-direction for flies presented with a light corridor in the presence (blue) or absence of wind. Right: Average heading inside the light corridor in the presence (blue) or absence of wind (black). n=14 flies (no wind), 15 flies (wind). ***p < 0.001 Details of statistical analyses and sample sizes are given in Table S1.

42

Extended Data Figure 5: Edge tracking is not the result of random exploration outside the plume. **(a)** Schematic of random-walk model. Left: individual outside trajectories from 40 flies tracking a vertical plume were decomposed into a series run lengths and turn angles using the Ramer-Douglas-Peucker algorithm to generate a library for generating synthetic trajectories with the same underlying statistics. Right: flowchart of how trajectories were simulated from this library. The fly was initiated at the plume's edge with an initial heading and run length matching

43

the distribution observed during actual fly exits from the plume. At each step, a run length, turn angle, and turn direction was chosen to update the new position (x,y) of the fly. The procedure was repeated until the simulated trajectories returned to the edge or traveled greater > 500 mm orthogonal to the plume's edge. The turn direction was biased by the wind direction as shown in the inset graph which compares the heading distributions for different upwind biases (a=0 to a=1.0). **(b)** Left: Distribution plots of initial headings for the three different plume geometries: 0-degree (light grey); 45-degree (dark grey) and 90-degree (black). Middle: distribution run lengths derived from the library of trajectories. Right: distribution of turn angles derived from the library of trajectories. **(c)** Relationship between upwind bias and upwind turn bias (a) for simulated and real flies. Upwind bias is defined as the distance traveled in the upwind direction divided by total path length. Note that real flies show an upwind bias of 0.35, which corresponds to an upwind turn bias (a=1.0). **(d)** Top: Average outside trajectories for flies (left) and simulated trajectories (right) tracking a vertical plume with different upwind biases (a=0, a=1.0). Note that in contrast to real flies, simulations lacking an upwind bias (a=0) never progress along the length of the plume. Simulations with a=1.0 make progress but lack directed returns. Because only simulated trajectories that successfully returned to the plume are included in these averages, they progressed further upwind than real flies but were less efficient as shown in (e). Bottom: Comparison of the inbound and outbound segments of outside trajectories (see Methods), defined as leading away from (outbound, black) or returning to (inbound, red) the point farthest from the plume in the crosswind direction for real flies (replotted from Fig. 1f), and simulated trajectories lacking an upwind bias (a=0) and with an upwind bias (a=1.0). **(e-h)** Comparison of real and simulated trajectories for different plume configurations: vertical plume (e, replotted from **Fig. 1g**), 45-degree plume (f), 90-degree plume (g), and jumping plume (h). Comparison of total path length as a function of distance in the perpendicular direction away from the plume for real flies (left column), model with a=0 (middle-left column), and model with a=1.0 (middle-right column). Right column compares the probability of returning for n consecutive outside bouts for real flies in black and random models shown in dark and light blue.
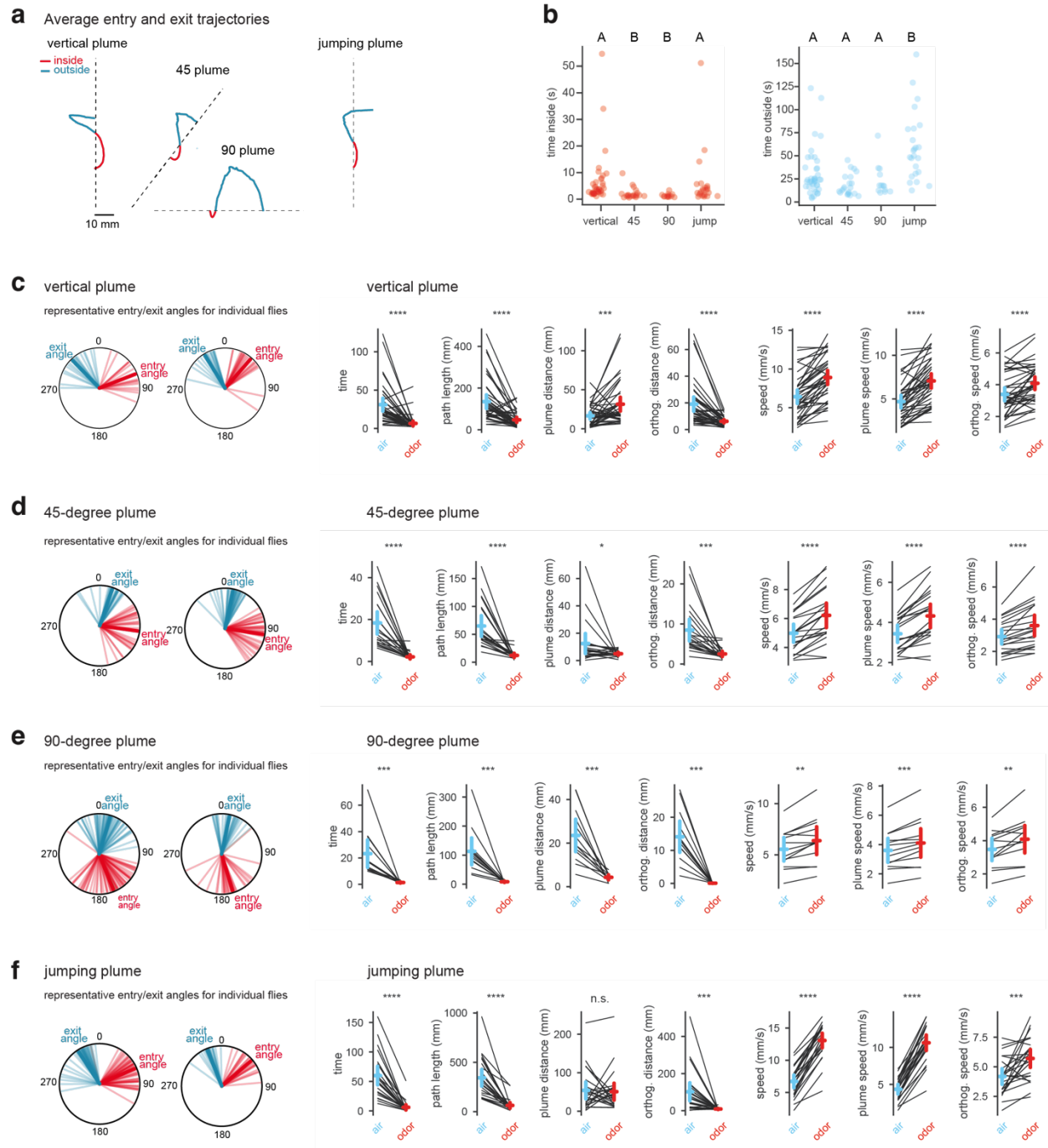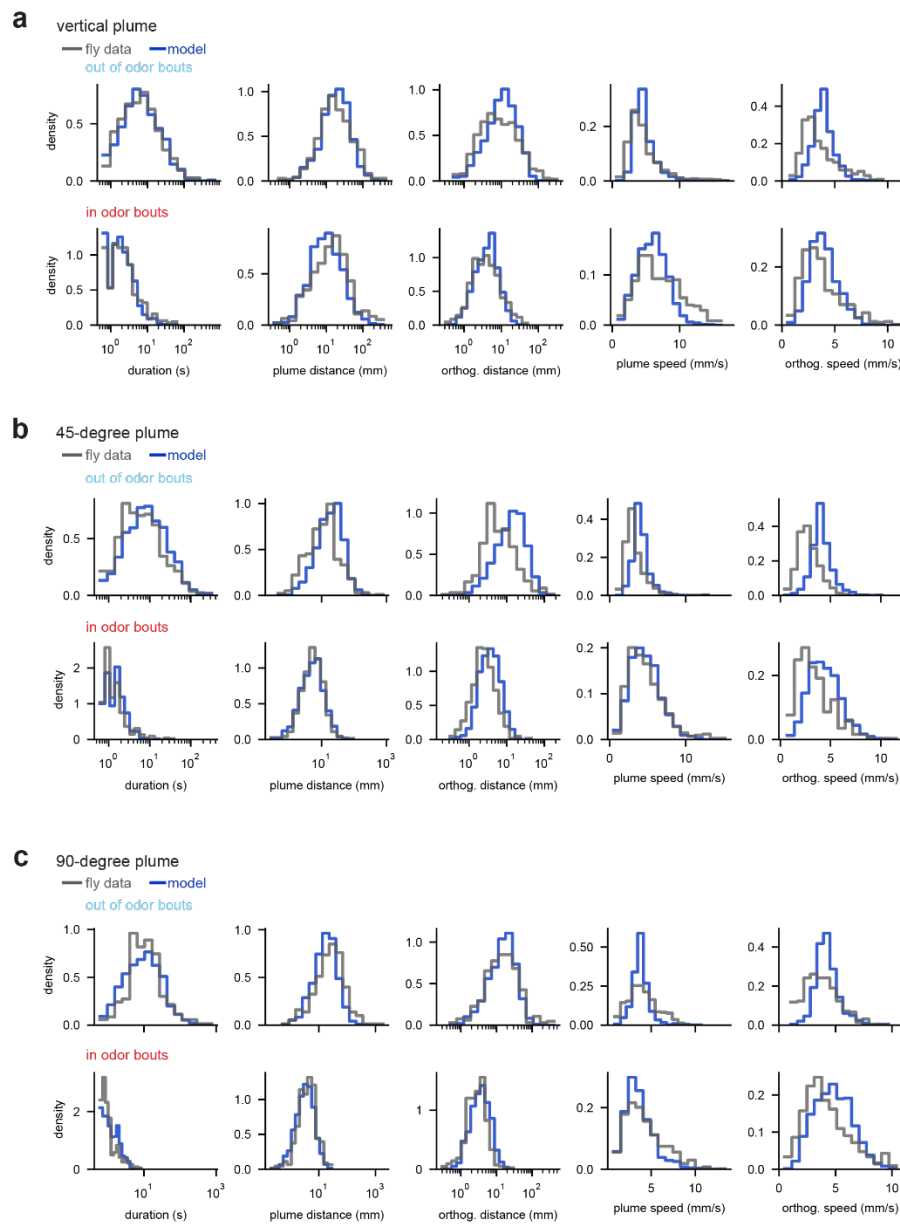
Extended Data Figure 6: Comparison of edge tracking of plumes with different orientations relative to the wind. **(a)** Comparison of aligned average trajectories for flies tracking indicated plume orientations, n=20-40 flies, replotted from Fig. 2e-h to highlight the variation in the inside (red) and outside (blue) trajectories of flies depending on the geometry of the plume they are tracking. **(b)** Comparison of time spent inside or outside the plume across different plume geometries, with each dot indicating the average of all trajectories for a single fly. n=20-40 flies. Letters denote statistically different groups (p < 0.05). **(c-f)** Left, entry (red) and exit (blue) angles for two representative individuals tracking the indicated plumes shows that flies use a restricted set of angles as they edge track. Right, comparison of behavioral metrics in clean air outside the plume (blue) and in odor (red) for indicated plumes. **(c)** 0-degree (with data replotted from Figure 1); **(d)** 45-degree; **(e)** 90-degree; **(f)** jumping plume. Each data point indicates the average for all inside or outside bouts for an individual trajectory. n.s., not significant, *p < 0.05, **p < 0.005, ***p < 0.001, ****p < 0.0001. Details of statistical analyses and sample sizes are given in Table S1.
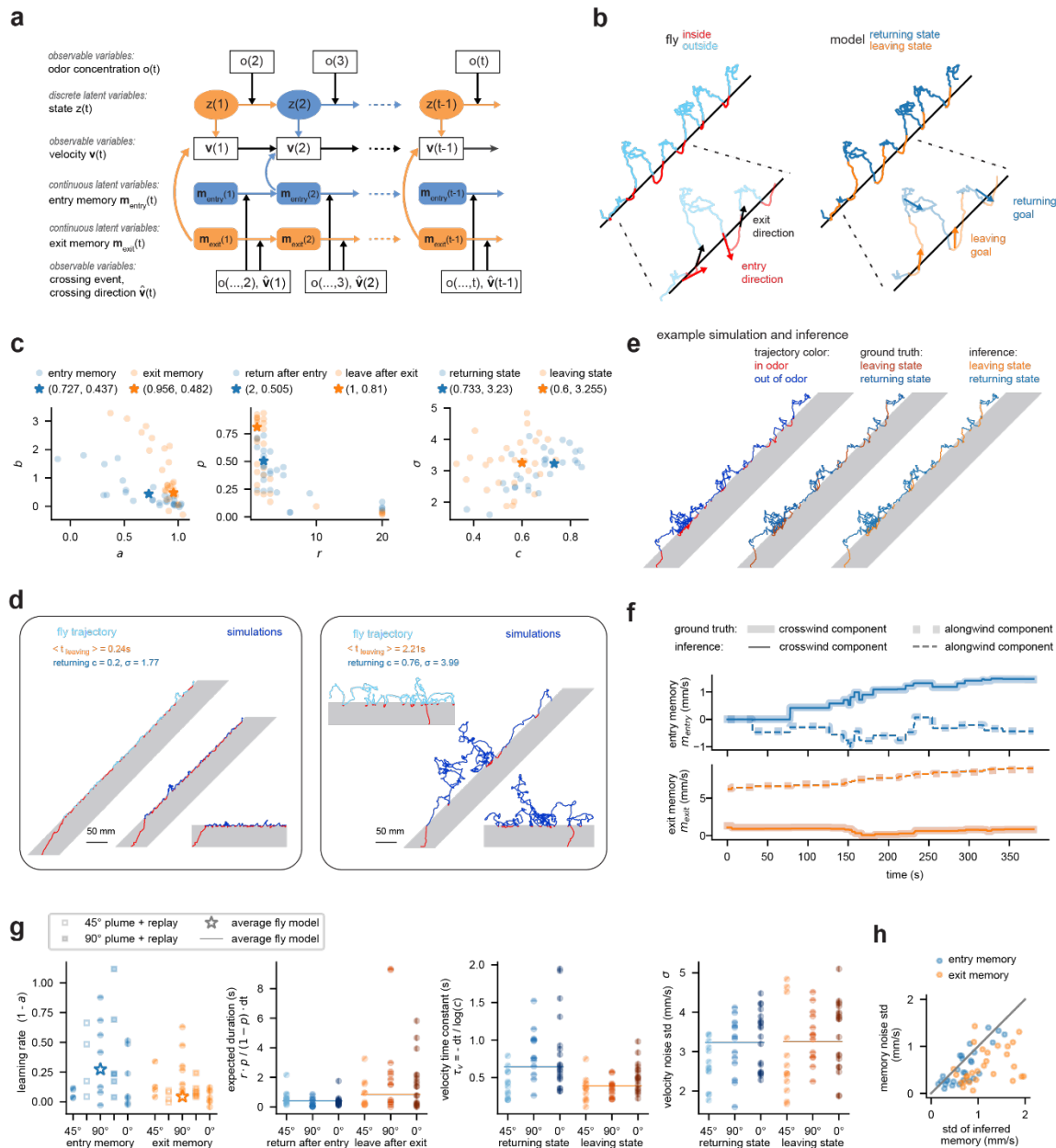
Extended Data Figure 7: A switching state space model for edge tracking. (a) Diagram of the switching state space model used to infer fly navigation states (discrete latent variables) and memories (continuous latent variables). The model also infers transition rates between states and parameters of the memory and velocity update rules. See Methods for details. **(b)** Representative example of a real fly trajectory with navigation states and memories inferred. Left: trajectory is colored according to when the fly is inside the plume (red) or outside the plume (light blue), with arrows indicating entry direction (red) and exit direction (black) as flies cross the plume's boundary. Right: The same fly trajectory colored according to leaving state (orange) and returning state (blue) with arrows indicating inferred leaving goal (orange) and returning goal (blue). Note that leaving and returning states are not equivalent to times when the fly is inside or outside the odor plume. **(c)** Scatter plots showing the distribution of parameters for the 28 trajectories (dots) from flies that made at least 30 returns which were used to train the model, and parameters for the average fly model (stars), see Methods for details. **(d)** Individual flies display heterogeneity in how closely they track the edge of the plume, reflected in distinct model parameters corresponding to different state transitions and velocity updates. Each box shows the representative trajectory for an individual fly (left, cyan) used to fit model parameters and two simulations (right, blue) for 45- and 90-degree plumes. All bouts inside the odor are shown in red. **(e)** Example inference of navigational states (right) compared with ground truth (middle) for a simulated

46

trajectory. **(f)** Example inference of memories (thin lines) compared with ground truth (thick lines) for the simulated trajectory in (e). **(g)** Parameter distributions across different experiments. The first panel shows the learning rate of 28 training trajectories (trajectories including replay experiment are shown by square markers). The second to last panels show state and velocity parameters for 46 edge tracking trajectories with at least 20 returns. **(h)** Joint distribution of the memory noise parameter and standard deviation of inferred memories for 28 training trajectories. Inferred memories here are the mean of variational distributions fitted to individual trajectories. Standard deviation of inferred memories is calculated as the geometric mean of crosswind component standard deviation and alongwind component standard deviation.

Extended Data Figure 8: Model captures the average statistics of edge tracking across different plume geometries. **(a-c)** Histograms comparing metrics of real and simulated fly trajectories tracking indicated plume orientations: **(a)** vertical (0-degree) (28 flies, 25 simulations), **(b)** 45-degree (24 flies, 25 simulations), and **(c)** 90-degree (20 flies, 25 simulations). These represent the same set of trajectories as in Figure 5c, d but now divided by plume geometry.

48
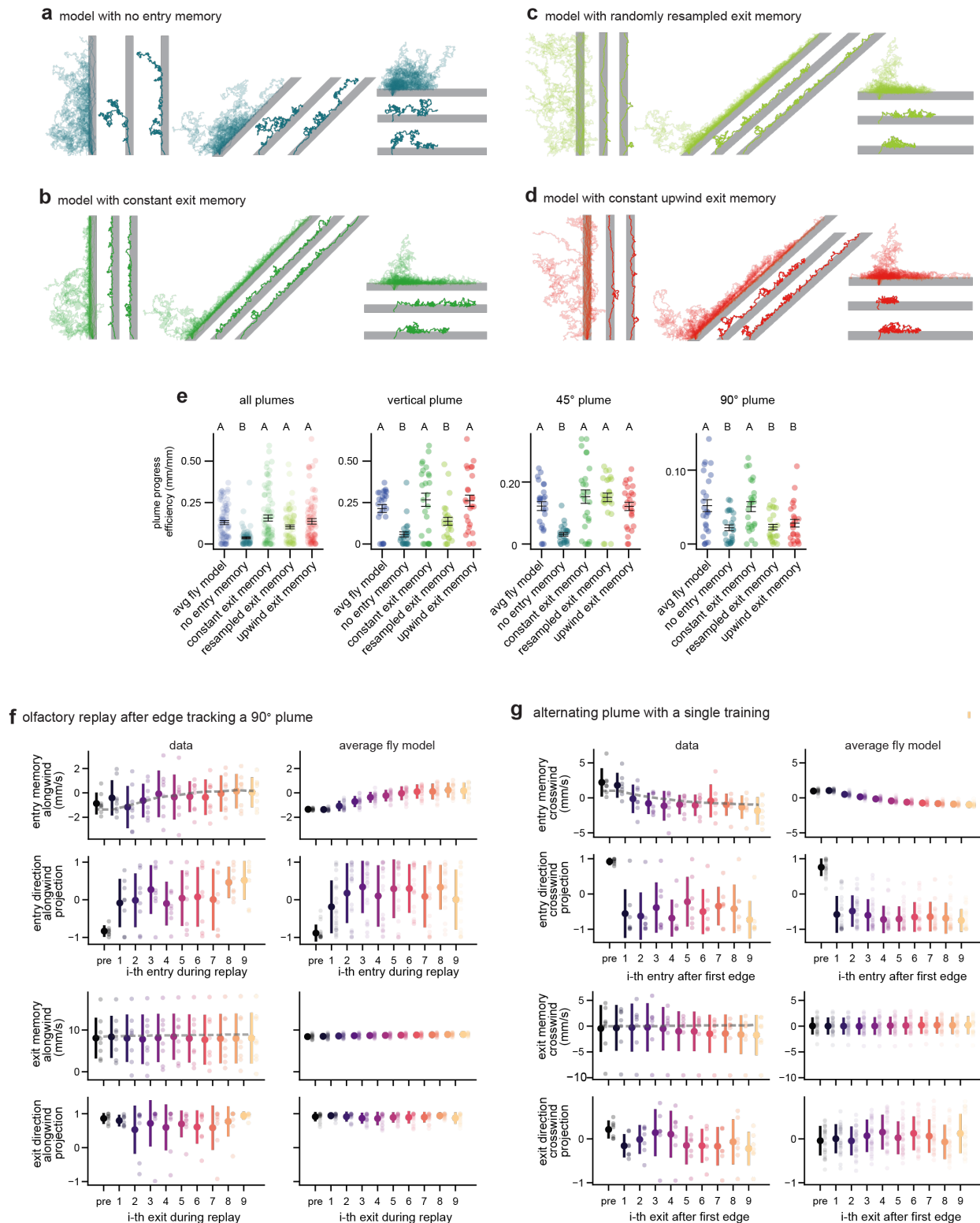
Extended Data Figure 9: The role of the entry and exit angle memory in the model. **(a)** Simulated trajectories tracking vertical, 45-degree and 90-degree plumes using a model where entry memory is maintained as a null vector. For each plume, two individual representative trajectories are shown (thick lines) along with an overlay of 25 trajectories. **(b)** Same as (a) but for simulated trajectories using a model that has a constant exit memory in the upwind direction with a random crosswind component. **(c)** Same as (a) but for simulated trajectories using a model

49

where the exit memory is resampled from the initialization distribution at each exit. **(d)** Same as (a) but for simulated trajectories using a model with a constant upwind exit memory. **(e)** Plume progress (distance between first and last exit divided by total path length) for indicated model variants. Letters denote statistically different groups (p < 0.05). Details of statistical analyses and sample sizes are given in Table S1. **(f)** Changes of the alongwind component of the entry angle memory, entry direction, exit memory and exit direction during olfactory replay after tracking a 90° plume (see **Fig 4b,c**). Results shown for trajectories with more than 9 entries during replay. Left: Entry and exit direction and inferred entry and exit angle memory for 8 real flies. Inferred memories are the mean of variational distributions fitted to individual trajectories. Dashed gray line indicates average from corresponding model trajectories plotted for comparison. Error bars show standard deviation. Right: Same as at left but plotted for 22 simulated trajectories. For simulations, entry and exit angle memory represent ground truth memory. **(g)** Changes of the crosswind components of entry memory, entry direction, exit memory and exit direction for alternating plume experiment (see **Fig 5e-f**) with a single operant training period. Results shown for trajectories with more than 9 entries after tracking the first edge. Left: Entry and exit direction and inferred entry and exit angle memory for 7 real flies. Dashed gray line represents average of the corresponding simulations plotted for comparison. Right: Same as at left but plotted for 28 simulated trajectories.
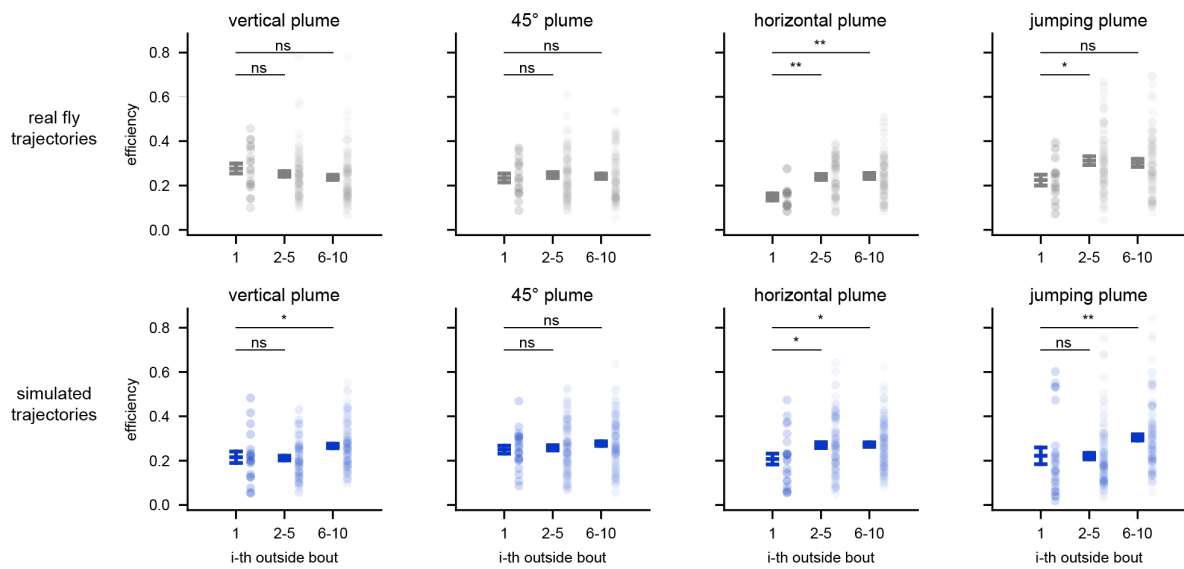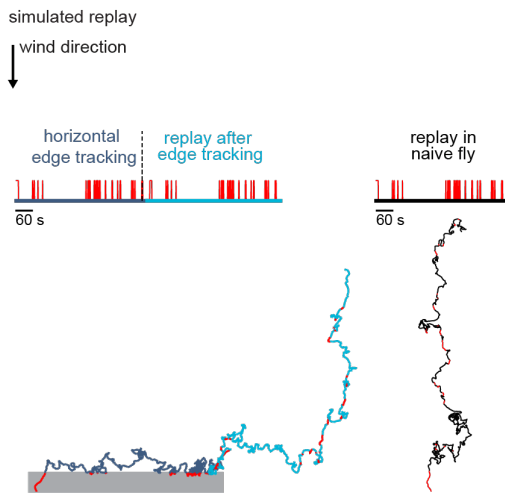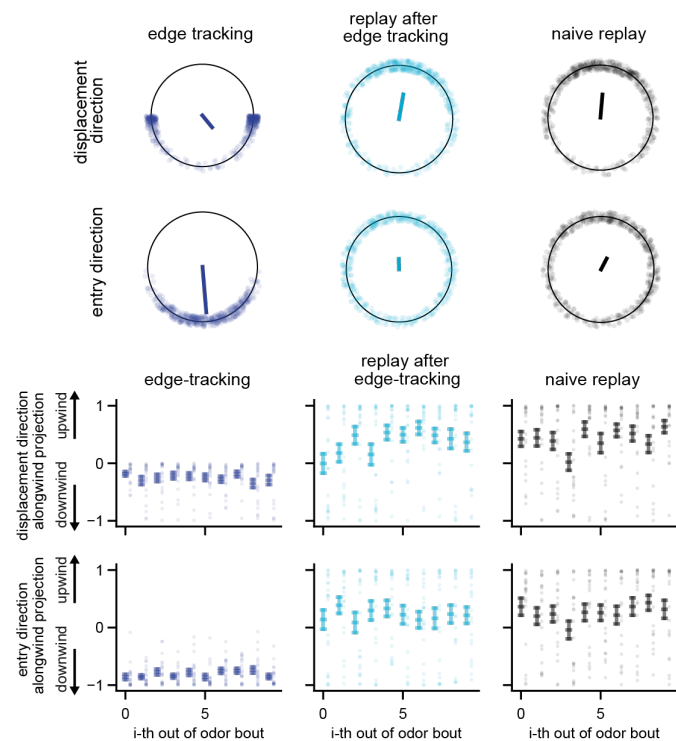
Extended Data Figure 10: Model of how flies modify their trajectories with experience. (a) Plots depicting the change in efficiency of outside bouts (distance perpendicular to edge divided by total path length) for real flies (top) and simulated trajectories (bottom) tracking different plume types (0-degree, 45-degree, 90-degree, and jumping plume). n=11-20 flies; 19-23 simulations. Each point represents the efficiency of a single bout with the lines representing the average value ± standard error. **(b)** Left: Representative simulation of the olfactory 'replay' experiment, showing simulated trajectory during edge tracking of a 90-degree plume (dark blue trace indicates outside the odor, red inside the odor), subsequent replay of the same odor sequence (light blue trace indicates outside the odor, red inside the odor) or replay of the same odor sequence to a naïve model (black trace indicates outside the odor, red inside the odor). Right, top: Polar plots showing the net displacement direction of simulated trajectories outside the odor and entry direction when they encounter the odor during edge tracking (left, dark blue),

replay (middle, cyan), or replay to naïve models (right, black). Each point represents a single bout. Solid lines represent the average vector. Right, bottom: changes of the alongwind projection of directions over outside bouts, error bars are standard error across n=21 simulations. For the alongwind projection, 1 denotes straight upwind and -1 denotes straight downwind. n.s., not significant p>0.05,* p <0.05, **p < 0.005. Details of statistical analyses and sample sizes are given in Table S1.
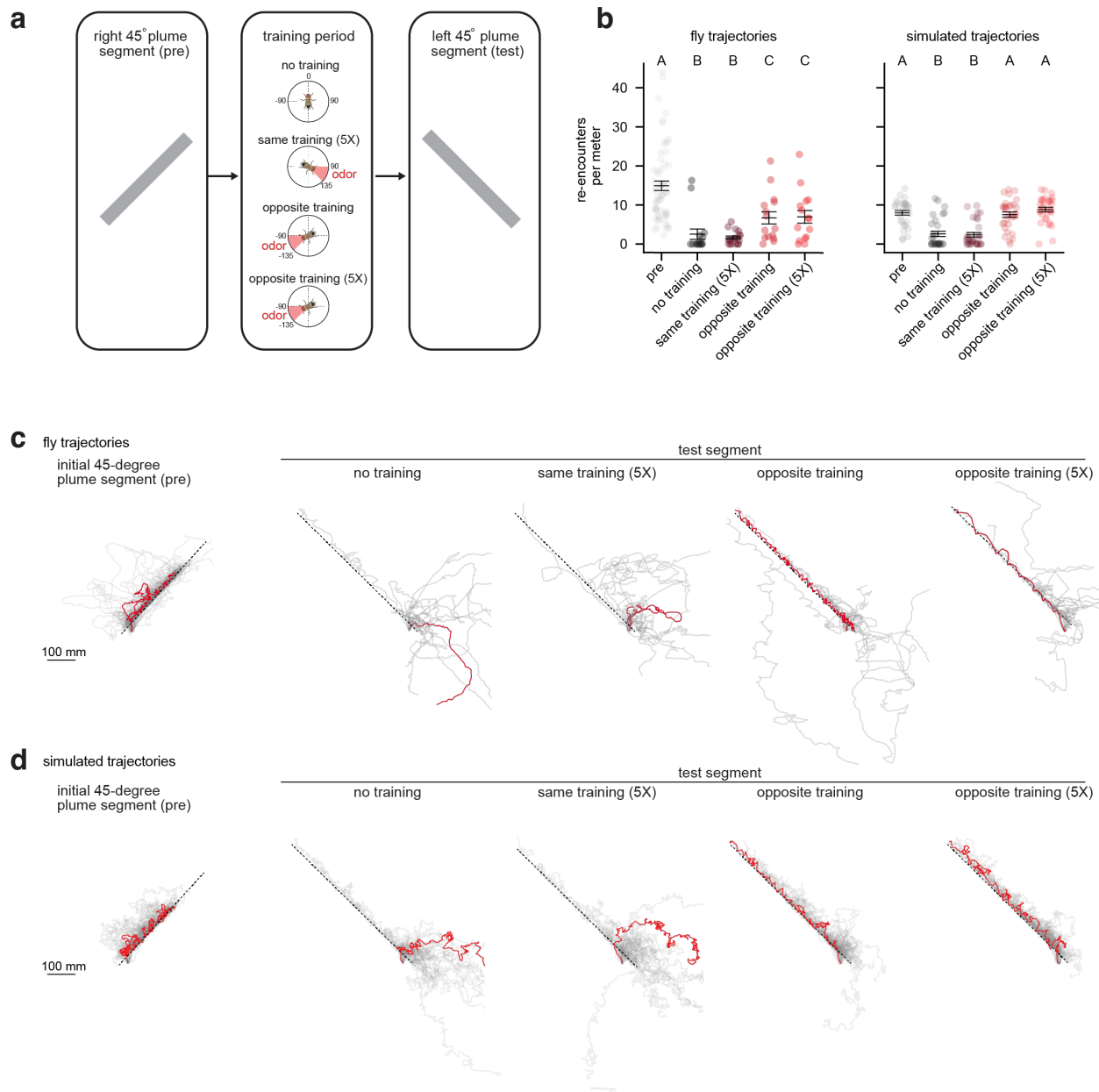
Extended Data Figure 11: Flies can be operantly trained to track plumes of different orientations. (a) Schematic of experimental protocol used to operantly train flies to track plumes in different orientations. After a 5-minute baseline period during which flies walked in clean air, they were given a 45° plume to navigate. Animals that edge tracked a plume for at least 250 mm were then subjected to one of four training conditions: No training, in which flies were immediately tested with a -45° plume in the opposite direction without reinforcement; Same training (5X), in which odor delivery was triggered when flies were heading in the same direction that would lead them back to the initial plume segment (e.g. the 90° to 135° sector), and ceased upon entering a 90° upwind exit zone (-45° to 45°) (training was repeated five times); Opposite training (1X), in which odor delivery was triggered when flies traveled in the direction (e.g. -90° to -135° sector) required to enter the second plume segment. Note that to enter the second plume segment flies must travel in the same direction as used for operant conditioning (-90° to -135°) and so effectively have a second operant training epoch; Opposite training (5X), consisting of five bouts of odor reinforcement triggered by entering the -90° to -135° sector required to enter the second plume segment. Plume orientations (e.g. whether the initial plume segment was oriented 45° or -45°) were interleaved across trials for consistency and the type of trial was defined in advance. **(b)** Comparison of the plume re-encounters per meter for the five conditions for real flies (left) and simulated trajectories (right). n=17 for same training, n=15 for no training and opposite training. n=31 simulations for each condition. **(c)** Overlaid trajectories for flies tracking the indicated plume segments: initial plume, no training, same training (5X), opposite training (1X), and opposite training (5X). Individual trajectories shown as thin black line with a single representative trajectory shown in red and plume's edge is depicted as dashed line. **(d)** Same as in (c) except for

simulated trajectories. Letters denote statistically different groups ($p < 0.05$). Details of statistical analyses and sample sizes are given in Table S1.

Table S1
Statistics and Sample Sizes

Figure	Group	Sample size	Statistical tests	p value	Additional notes
1d	in air, in odor for flies tracking a vertical plume	n = 40 flies	Paired t-test	p=0.00096	plume distance
				p=2.60e-06	orthogonal distance
			Wilcoxon signed rank	p=4.60e-10	speed
				p=4.60e-10	plume speed
				p=8.85e-06	orthogonal speed
1d	outbound, inbound	n = 40 flies	Wilcoxon signed rank	p=1.82e-12	angle
			Paired t-test	p=0.00014	distance
1g	pathlength for outside bouts real flies (1) simulated trajectories, a=0 (2) simulated trajectories, a=1 (3)	n=755 outside trajectories from 40 flies or 755 simulated trajectories	Kruskal-Wallis Dunn's post hoc test	(1, 2) p=3.65107e-7 (1, 3) p=2.131035e-4 (2, 3) p=0.562384	pathlength for outside bouts
2j	traveling direction of flies after plume disappears	n=12 flies (0°) n=11 flies (45°) n=6 flies (90°)		p= 2.0e-09	0° vs 90 °
				p= 5.3e-08	0° vs. 45°
				p=0.05	45° vs. 90°
3f	EPG >GtACR	n = 12 flies	Wilcoxon signed rank	p=0.0049	660 nm LED on vs. LED off
	>GtACR	n = 6 flies	Wilcoxon signed rank	p=0.5625	
	EPG >GtACR	n = 12 flies	paired t-test	p=0.0087	
	>GtACR	n = 6 flies	Wilcoxon signed rank	p=0.7108	
5h	flies/model with or without operant training	n = 15 flies	Kruskal-Wallis H-test	p = 0.00463	plume re-encounters plume with or without operant training
		n = 31 simulations	Kruskal-Wallis H-test	p = 1.07e-05	
ED3b	tracking a vertical plume of constant, increasing or decreasing odor concentration	n=12 flies	Wilcoxon signed rank	p>0.05	inside speed, outside speed, inside plume distance, outside plume distance, inside pathlength, outside pathlength, inside time, outside time
ED 3d	tracking a vertical plume of constant, increasing or decreasing odor concentration	n=12 flies	Wilcoxon signed rank	p>0.05	inside speed, outside speed, inside time, outside time, inside pathlength, outside pathlength
ED 4e	Orco>Chrimson flies wind, no wind	n=14 flies (no wind) n=15 flies (wind)	Student's t-test	p < 0.001	net displacement in Y-direction
ED 5d	inbound, outbound for real and simulated trajectories	flies			
		simulations			
		simulations			
ED 6b	flies tracking plumes of different orientations	n = 40 flies (0°) n = 21 flies (45°) n = 20 flies (90°)	Kruskal-Wallis Dunn's post hoc test	(0, 45) p=0.000150 (0, 90) p=0.000008 (0, jump) p=0.992539 (45, 90) p=1.00000 (45,jump) p=0.055501 (90, jump) p=0.003577	time of inside bouts

		n = 24 flies (jump)		(0, 45) p= 0.173647 (0, 90) p=1.00000 (0, jump) p= 0.002681 (45, 90) p=1.00000 (45,jump) p=0.000003 (90, jump) p= 0.002253	time of outside bouts
ED 6c	in air, in odor flies tracking a vertical plume	n=40 flies	Paired-t	1.66e-06	time
			Paired-t	1.39e-06	path length
			Paired-t	0.00096	plume distance
			Paired-t	2.60e-06	orthogonal distance
			Wilcoxon signed rank	4.60e-10	speed
			Wilcoxon signed rank	1.82e-11	plume speed
			Wilcoxon signed rank	8.85e-06	orthogonal speed
ED 6d	in air, in odor flies tracking a 45-degree plume	n=21 flies	Paired-t	8.02e-06	time
			Paired-t	2.38e-05	path length
			Wilcoxon signed rank	0.0175467	plume distance
			Paired-t	0.002057	orthogonal distance
			Wilcoxon signed rank	2.86e-06	speed
			Wilcoxon signed rank	4.77e-06	plume speed
			Wilcoxon signed rank	4.77e-06	orthogonal speed
ED 6e	in air, in odor flies tracking a 90-degree plume	n=13 flies	Paired-t	0.000724	time
			Wilcoxon signed rank	0.000244	path length
			Wilcoxon signed rank	0.000244	plume distance
			Wilcoxon signed rank	0.000244	orthogonal distance
			Wilcoxon signed rank	0.00244	speed
			Wilcoxon signed rank	0.000732	plume speed
			Wilcoxon signed rank	0.002441	orthogonal speed
ED 6f	in air, in odor flies tracking a jumping plume	n=21 flies	Paired-t	1.67e-07	time
			Paired-t	2.48e-05	path length
			Paired-t	0.882320	plume distance
			Wilcoxon signed rank	0.000908	orthogonal distance
			Wilcoxon signed rank	1.19e-07	speed
			Wilcoxon signed rank	1.19e-07	plume speed
			Wilcoxon signed rank	0.000568	orthogonal speed
ED 9e	average fly model (1) model w/ no entry memory (2) model w/ constant exit memory (3) model w/ resampled exit memory (4) model w/ upwind exit memory (5)	n= 75 simulations for each model	Kruskal-Wallis Dunn's post hoc test	(1, 2) p=7.931e-08 (1, 3) p=0.9079 (1, 4) p=0.1889 (1, 5) p=0.7689 (2, 3) p=4.150e-08 (2, 4) p=5.014e-05 (2, 5) p=3.879e-07 (3, 4) p=0.1529 (3, 5) p=0.6822 (4, 5) p=0.3078	All plumes
ED 9e	average fly model (1) model w/ no entry memory (2) model w/ constant exit memory (3)	n= 25 simulations for each model	Kruskal-Wallis Dunn's post hoc test	(1, 2) p=3.753e-04 (1, 3) p=0.6436 (1, 4) p=0.09204	vertical plume

56

	model w/ resampled exit memory (4) model w/ upwind exit memory (5) (5)			(1, 5) p=0.4488 (2, 3) p=5.831e-05 (2, 4) p=0.06119 (2, 5) p=1.601e-05 (3, 4) p=0.03176 (3, 5) p=0.7686 (4, 5) p=0.0146	
ED 9e	average fly model (1) model w/ no entry memory (2) model w/ constant exit memory (3) model w/ resampled exit memory (4) model w/ upwind exit memory (5)	n= 25 simulations for each model	Kruskal-Wallis Dunn's post hoc test	(1, 2) p=1.291e-04 (1, 3) p=0.4462 (1, 4) p=0.2289 (1, 5) p=0.9829 (2, 3) p=4.434e-06 (2, 4) p=4.870e-07 (2, 5) p=1.408e-04 (3, 4) p=0.6589 (3, 5) p=0.4335 (4, 5) p=0.2207	45-degree plume
ED 9e	average fly model (1) model w/ no entry memory (2) model w/ constant exit memory (3) model w/ resampled exit memory (4) model w/ upwind exit memory (5)	n= 25 simulations for each model	Kruskal-Wallis Dunn's post hoc test	(1, 2) p=6.733e-03 (1, 3) p=0.7282 (1, 4) p=1.246e-02 (1, 5) p=4.644e-02 (2, 3) p=2.234e-03 (2, 4) p=0.8330 (2, 5) p=0.4.725 (3, 4) p=4.421e-03 (3, 5) p=1.934e-02 (4, 5) p=0.6117	90-degree plume
ED 10a	path efficiency as a function of outside bout for real flies first outside bout (1) avg 2-5 outside bout (2) avg 6-10 outside bout (3)	n= 20 flies	the Mann-Whitney U rank test	(1, 2) p=0.2327 (1, 3) p=0.0676	Vertical plume
		n= 17 flies	the Mann-Whitney U rank test	(1, 2) p=0.8734 (1, 3) p=0.8224	45-degree plume
		n= 11 flies	the Mann-Whitney U rank test	(1, 2) p=2.362e-03 (1, 3) p=1.457e-03	90-degree plume
		n= 14 flies	the Mann-Whitney U rank test	(1, 2) p=0.03641 (1, 3) p=0.06033	jumping plume
	path efficiency as a function of outside bout for simulations first outside bout (1) avg 2-5 outside bout (2) avg 6-10 outside bout (3)	n= 19 simulations	the Mann-Whitney U rank test	(1, 2) p=0.90005 (1, 3) p=0.044720	Vertical plume
		n= 22 simulations	the Mann-Whitney U rank test	(1, 2) p=0.96722 (1, 3) p=0.28390	45-degree plume
		n= 23 simulations	the Mann-Whitney U rank test	(1, 2) p=0.03325 (1, 3) p=0.15180	90-degree plume
		n= 23 simulations	the Mann-Whitney U rank test	(1, 2) p=0.44807 (1, 3) p=3.6380e-03	jumping plume
ED 11b	flies with or without operant training pre (1) no training (2) opposite training, 5X (3) same training, 1X (4) same training, 5x (5)	n=62 flies (initial segment) n=17 flies (same training) n=15 flies (no training) n=15 flies (1X opposite training) n=15 flies (5X opposite training)	Kruskal-Wallis Dunn's post hoc test	(1, 2) p=1.2915e-08 (1, 3) p=1.1801e-09 (1, 4) p=2.4689e-03 (1, 5) p=2.9562e-03 (2, 3) p=0.93497 (2, 4) p=0.036068 (2, 5) p=0.032403 (3, 4) p=0.024944 (3, 5) p=0.022205 (4, 5) p=0.96551	fly trajectories re-encounters per meter
ED 11b	model with or without operant training pre (1) no training (2) opposite training, 5X (3) same training, 1X (4) same training, 5x (5)	=31 simulations for each condition	Kruskal-Wallis Dunn's post hoc test	(1, 2) p=1.0397e-06 (1, 3) p=8.4910e-07 (1, 4) p=0.58465 (1, 5) p=0.51096 (2, 3) p=0.96829 (2, 4) p=1.4420e-05 (2, 5) p=3.0019e-08 (3, 4) p=1.2026e-05 (3, 5) p=2.3903e-08 (4, 5) p=0.22861	model trajectories re-encounters per meter